Electronics and Electrical Engineering

AIMS Electronics and Electrical Engineering, 10(1): 92–128.
DOI: 10.3934/electreng.2026005
Received: 16 June 2025
Revised: 21 October 2025
Accepted: 13 November 2025
Published: 20 January 2026

https://www.aimspress.com/journal/ElectrEng

Research article

Electronic components and key algorithms for a prototype drone: Economic and sustainability advantages

Luigi Bibbo[1], Emanuela Genovese[2], Clemente Maesano[3], Sonia Calluso[3], Gabriele Barrile[4], Giuseppe Maria Meduri[1], Giuliana Bilotta[1] and Vincenzo Barrile[2,*]

[1] Department of Architecture and Design (DAeD) – "Mediterranea" University of Reggio Calabria, Via dell'Università, 89124, Reggio Calabria, (Italy); luigi.bibbo, giuliana.bilotta, giuseppemaria.meduri@unirc.it

[2] Department of Civil, Energy, Environment and Materials (DICEAM) – "Mediterranea" University of Reggio Calabria, Via Zehender, 89124, Reggio Calabria, (Italy); emanuela.genovese, giuseppemaria.meduri, giuliana.bilotta, vincenzo.barrile@unirc.it

[3] Department of Civil, Building and Environmental Engineering (DICEA) – "Sapienza" University of Rome, Via Eudossiana, 18, 00184, Rome, (Italy); sonia.calluso, clemente.maesano@uniroma1.it

[4] LUISS Libera Università Internazionale degli Studi Sociali Guido Carli Viale Pola 12, 00198 Roma, (Italy); gabriele.barrile@studenti.luiss.it

*** Correspondence:** Email: vincenzo.barrile@unirc.it; Tel: +39 0965 1692414.

Abstract: In recent years, the use of drones for cargo transport has experienced rapid development, driven by the need to reduce the environmental impact of traditional delivery systems and improve access to essential services, particularly in complex urban environments. In this study, we aimed to present the first experimental results for the development of a drone prototype characterized by low energy consumption and the integration of advanced technologies, with attention to the electronic components and embedded algorithms. The combination of cutting-edge technologies with such advanced algorithms enabled us to witness a reduction in the carbon footprint in terms of resource optimization, due especially to the neural network algorithms suitable for path analysis and obstacle detection, and the cutting-edge processor that enables us to manage and analyze the data derived from the different sensors. The design of this drone focuses on minimizing environmental impact through optimized energy resources by using high-efficiency components, including brushless DC motors and lithium polymer (LiPo) batteries integrated with perovskite photovoltaic cells that extend flight autonomy while reducing dependence on traditional energy sources. The drone's body, made of

lightweight and durable materials, improves aerodynamic efficiency without compromising structural strength. Advanced artificial intelligence algorithms optimize flight paths, prevent collisions, and adapt dynamically to environmental conditions. Thanks to computing platforms such as the NVIDIA Jetson Nano and equipped with advanced sensors like LiDAR, accelerometers, and gyroscopes, the drone processes data in real-time, enhancing its autonomous operation and ensuring precise and stable navigation. The proposed prototype represents a significant step toward a future where technology supports sustainability, providing innovative solutions for modern society's needs aiming to reduce urban traffic and pollutant emissions, offering an efficient and ecofriendly solution for urban logistics.

Keywords: UAVs; eco-sustainable UAV; electronics components; perovskite; artificial intelligence (AI); prototype

1. Introduction

In recent years, Unmanned Aerial Vehicles (UAVs), commonly known as drones, have emerged as a revolutionary technology in the delivery industry. Their ability to navigate urban traffic easily and quickly reaching remote or inaccessible areas provides a significant advantage over traditional vehicles. Drones are no longer just a futuristic concept; they are becoming a practical reality in freight transport. Companies grappling with supply chain issues and driver shortages recognize this technology's numerous benefits, including reduced personnel costs, the ability to operate continuously for 24 hours, fewer infrastructure challenges, and decreased CO_2 emissions due to the use of electric-powered drones. Industry developments are highlighted, such as UPS and DHL acquiring vertical takeoff aircraft and Poste Italiane's experiments with drones for carrying light cargo. Notable developments include UPS, which has acquired ten vertical takeoff aircraft capable of transporting 635 kg over 450 km, set to be operational in 2024. Similarly, DHL has purchased aircraft that can carry 1,200 kg over 800 km, scheduled to be operational in California in 2024. Poste Italiane is also experimenting with drones that can carry 100 kg over short distances.

The expansion of the UAV sector can be attributed in part to significant improvements in electronic components. For instance, using more batteries and applying supercapacitors can help offset battery limitations by providing an energy boost as needed, such as during takeoff [1]. Integrating photovoltaic cells can extend battery life by using solar energy under bright conditions [2]. Improvements in motors are also crucial, as one of the major challenges for drones is maintaining consistent torque in brushless DC (BLDC) motors to sustain high thrust and achieve fault tolerance, enhancing operational continuity [3]. For example, Yasa developed an efficient BLDC motor explicitly designed for UAVs, with the following specifications: Power output of 650 watts, maximum speed of 3500 rpm, Kv rating of 225 Kv, and a traction force capacity of 5 kg [4]. Moreover, Deepak et al. investigated design factors in drone delivery systems and conducted comparisons to determine the optimal BLDC motor configuration [5].

Significant advancements in drone manufacturing can be attributed to integrating sensors and microcontrollers. Most drones are equipped with GPS sensors to accurately determine their location and accelerometers and gyroscopes to monitor orientation, angular velocity, and acceleration [6]. Additionally, many drones are now fitted with cameras, either RGB or multispectral [7], Light Detection and Ranging (LiDAR) sensors, to create detailed 3D maps [8] and chemical sensors, which

can identify gas leaks [9]. A comprehensive review by Wei et al. discusses anticollision technologies for UAVs, which are essential for ensuring flight safety [10]. Another critical factor that ensures optimal flight performance is the drone's frame. A noteworthy study by Harika et al. explored how the quality of materials affects the performance of x-shaped drones [11]. Their proposed drone prototype incorporates the latest technological innovations, addressing specific logistics and goods delivery needs while considering environmental impacts. The primary goal is to achieve high operational reliability, maximize flight range, and enhance aerodynamic performance.

Studies have demonstrated that integrating advanced technologies into drones has led to significant efficiency gains. For instance, using perovskite photovoltaic cells in drones has been shown to reduce total energy consumption by 20% compared to drones powered solely by LiPo batteries. This finding is supported by studies such as that of Sampaio Saloio et al. [12], which indicated an increase in flight autonomy of up to 7 hours and 34 minutes thanks to incorporating solar cells. Additionally, the adoption of brushless DC motors, known for their high efficiency and long lifespan, has further enhanced the energy efficiency of drones, leading to reduced energy consumption during flight [4]. The integration of perovskite photovoltaic cells significantly extends the flight range, making drones more suitable for long duration missions. Furthermore, using artificial intelligence algorithms to optimize flight paths and prevent collisions has improved operational efficiency, energy conservation, and increased flight safety. For example, a study by Pal et al. [13] examined the applications of drones utilizing artificial intelligence and green computing technologies across industries. The findings showed that integrating AI with UAVs significantly boosts operational efficiency and safety, making aircraft systems more innovative and responsive. Annadata et al. [14] proposed a framework for implementing Tiny Machine Learning (TinyML) on autonomous drones to enhance precision agriculture. Optimizing TinyML models and adopting adaptive route planning improved drone energy and operational efficiency while reducing the computational resources required. Additionally, researchers investigated the energy efficiency of multirotor drones, revealing that energy optimization per meter traveled per unit mass remains consistent across vehicle mass conditions, including payloads [15]. This underscores the importance of optimizing flight parameters to enhance overall energy efficiency. Real-world experiences from companies like Keltbray [16], a leading construction engineering company, have demonstrated that utilizing drones for inspection and monitoring can double operational efficiency and reduce carbon emissions. Li et al. [17] proposed a framework for traffic management and resource allocation specifically for UAV-based parcel delivery in low-altitude urban areas. The research demonstrated that effective traffic management models can optimize airspace utilization and minimize route conflicts, improving the overall efficiency of drone delivery operations. The developed drone represents a significant advancement in sustainable transportation solutions. By utilizing high-efficiency brushless DC motors and lithium polymer (LiPo) batteries, the drone achieves low power consumption. Testing has shown that the drone consumes an average of 0.08 MJ/km, producing approximately 70 grams of CO_2 emissions per delivery. This is considerably lower than the 500 grams of CO_2 emitted by a diesel van over the same distance [18].

A comprehensive systematic review of sustainability assessments related to drone technologies [19], encompassing the drone as a product and the delivery service it provides, indicates that the use of electric drones in freight transport could reduce up to 12.2 million tons of CO_2 emissions each year by 2045. Additionally, drones can reduce medical delivery times in rural areas by as much as 85%, improving access to essential services. In agriculture, drones employed for multispectral surveys and precision techniques can decrease annual water consumption by up to 96%, reduce pesticide usage by 10%, and lower CO_2 emissions by up to 99% [20]. Bao et al. [21] explored the

integration of drones and trucks in logistics to tackle the challenges of last mile delivery. Their study highlights this collaborative model's environmental and economic benefits, including a 20% reduction in carbon emissions and a 20–30% decrease in costs compared to traditional fuel-powered truck fleets.

Furthermore, the continuous upgrading of electronic components to be more compact and energy efficient, and in Artificial Intelligence, with the development of more complex and accurate algorithms, are boosting the drone's market sector, which is beginning to be more attractive to the investors.

In this context, we aim to create a prototype that arises from an in-depth analysis of the context, integrating the most innovative electronic components, which ensure the most optimal resource allocation and use, in particular the electric capacity, together with cutting-edge AI algorithms that can make the drone reactive to the surrounding environment and to adjust its performance according to the data collected from the internal sensors integrated into a single solution. The developed prototype of the drone must possess specific characteristics that meet the requirements of sustainable transport of goods. This includes the integration of high efficiency brushless DC motors, lithium polymer (LiPo) batteries, and perovskite photovoltaic cells to extend flight range and reduce reliance on traditional energy sources. The drone's body, made of lightweight and durable materials, improves aerodynamic efficiency without compromising structural strength. Advanced artificial intelligence algorithms optimize flight paths, prevent collisions, and adapt dynamically to environmental conditions. Using computing platforms, such as the NVIDIA Jetson Nano, the drone processes data in real-time, enhancing its autonomous operation. Equipped with advanced sensors like LiDAR, accelerometers, and gyroscopes, the drone ensures precise and stable navigation.

To this end, our objectives of this study are:

- To present the first experimental results for the development and evaluation of a prototype drone designed for the sustainable transport of light goods in urban environments.
- To integrate electronic technologies with artificial intelligence algorithms for flight path optimization, collision avoidance, and image enhancement.

The relevance of this research lies in the growing need for sustainable transport solutions and the urgent need to reduce CO_2 emissions and the environmental impact of traditional delivery systems. The use of drones for urban logistics offers an efficient and environmentally friendly solution, providing fast and safe deliveries, which is particularly useful for the urgent transport of medicines and other essential goods. This prototype represents a significant step towards a future in which technology becomes a strategic ally of sustainability, offering innovative and responsible solutions for the needs of modern society.

In terms of sustainability, the drone's electric propulsion system and incorporation of renewable energy sources such perovskite photovoltaic cells significantly lower energy usage, noise pollution, and greenhouse gas emissions. Furthermore, the drone's construction's use of recyclable, lightweight materials encourage a circular economy strategy, lowering the drone's environmental impact over time.

In terms of economics, the deployment of self-governing drone delivery systems offers a feasible blueprint for sustained cost reduction. Particularly in industries with high delivery volumes, lower operating costs, due to lower fuel consumption, fewer maintenance requirements, and the removal of driver wages, enable scalability and affordability. Drones can also improve customer satisfaction and supply chain logistics by facilitating quick last-mile deliveries, which will open new business options and help sustainable urban economies flourish.

2. Materials and methods

The methodology is focused on the design and analysis of a drone prototype integrating advanced electronic components, such as brushless DC motors, lithium polymer (LiPo) batteries, and perovskite photovoltaic cells. Each of these components has been selected for their high efficiency and sustainability, ensuring that the drone operates with minimal environmental impact. Brushless DC motors are chosen for their high efficiency and reliability, which are crucial for maintaining constant torque and thrust. LiPo batteries are selected for their high energy density and long lifespan, which extend the drone's flight range. Perovskite photovoltaic cells have been integrated to harness solar energy [22,23], further improving the drone's energy efficiency and reducing its reliance on traditional energy sources. AI algorithms enable the drone to adapt dynamically to changing environmental conditions, ensuring safe and efficient operation. The integration of AI facilitates real-time data processing and decision-making, enhancing the drone's autonomous capabilities.

The methodological approach focuses on the integration of those components that, due to their high efficiency and sustainability, can ensure that the drone makes safe deliveries with minimal environmental impact. In the articulation of this study, a detailed description of the different phases is provided, as illustrated in Figure 1, highlighting how innovative technologies can be integrated to create an efficient and sustainable drone.

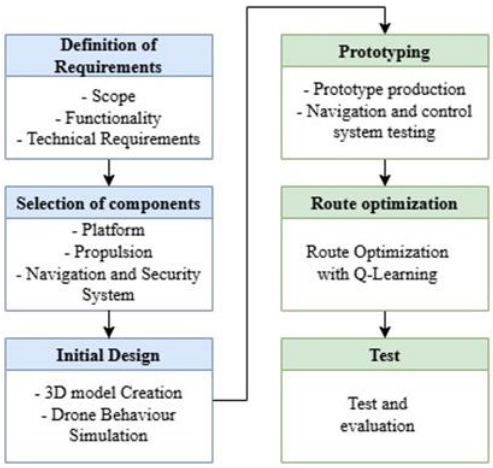

Figure 1. Workflow of the drone development methodology. The diagram illustrates the sequential phases of the project, including CAD-based structural design, selection and integration of electronic components, AI algorithm implementation, and experimental validation. Each step is informed by performance simulations and real-world testing to ensure energy efficiency and autonomous navigation capabilities.

2.1. Drone structure

2.1.1. Frame

The frame is printed in 3D and made of polylactic acid (PLA). PLA is an aliphatic polyester made from renewable sources, such as corn [21,24,25]. Standard PLA is not very resistant to heat and UV rays, which can lead to warping and degradation over time when exposed to outdoor

conditions. However, there are variants of PLA, such as carbon fiber-filled PLA (HTPLACARBON), which offer greater heat resistance.

PLA is the first natural fiber that can be melted [26,27]. Under optimal conditions, PLA is compostable and can be degraded by hydrolysis [28,29]. To make PLA, it is necessary to extract starch from corn or sugar from sugar beet. Other plants that can be used for starch extraction are rice, wheat, rye, and sweet potato. Sugar can also be made from whey or molasses [30–32]. Starches are converted, by enzymatic hydrolysis, into fermentable sugars (such as glucose and dextrose). Microorganisms, through a fermentation process, break down sugar into smaller species known as lactic acid [2,33]. PLA from lactic acid can be obtained via two processes: The first is the polycondensation of lactic acid under vacuum and high temperature, using a solvent to extract the water produced by the condensation reaction [34]. The second method is ring polymerization of a cyclic lactic acid dimer, which uses milder conditions. Mabbrur et al. [35] determined some mechanical properties of PLA:

- Polymer density: 1210-1250 kg/m ^{3}
- Tensile strength: 2160 x 10^6 N/m^2
- Tensile modulus: 0.353.5 GPa
- Specific tensile strength: 16.848 kNm/kg
- Specific tensile modulus: 2802800 kNm/kg
- Melting Point: 150162 ℃.

As industry advances, there is a potential shift toward more ecofriendly materials. A promising alternative to PLA is mushroom mycelium, which can be coated with other bioplastic materials, opening new avenues for sustainable drone construction.

Standard PLA tends to be less durable than other materials such as ABS or PETG, especially under conditions of mechanical stress or prolonged exposure to the atmospheric elements. Reinforced variants, such as PLA with carbon fibers, can significantly improve durability. To improve the strength and durability of the frame, it is advisable to increase the thickness of the walls. Generally, for PLA 3D prints that require strength and durability, a wall thickness of 1.22 mm is recommended.

Since the drone we developed must withstand a total weight of about 14 kg, it is necessary to opt for wall thickness toward the upper end of 2 mm. Applying a layer of epoxy resin can significantly improve resistance to impact and external influences. To achieve good protection, a layer of epoxy resin of about 12 mm should be sufficient. Although PLA is a biopolymer derived from renewable sources such as corn or sugar beet and is biodegradable under industrial composting conditions, the inclusion of carbon fibers and the application of an epoxy coating significantly reduce its end-of-life biodegradability. From a sustainability standpoint, this configuration offers environmental advantages in terms of energy efficiency and lower carbon footprint during manufacturing and operation, even though its post-use recyclability is limited.

The structure, in PLA, is X-shaped reticular, reinforced with carbon fibers, with walls 2 mm thick and with epoxy resin protection measures 700 x 700 x 250 mm. The weight of the structure is about 3.5 kg. The total weight of the drone resulting from the combination of the components of the prototype with a transportable weight of about 5 Kg is about 14 kg.

To support the decision of using PLA instead of other materials, according to [36], the following table shows the characteristic of PLA compared with the characteristic of Polyethylene Terephthalate Glycol or PETG, and Acrylonitrile Butadiene Styrene or ABS.

Table 1. Properties of PLA, PETG and ABS in 3D printing.

PRINT SPECIFICATION	PLA	PETG	ABS
Extrusion Temperature (℃)	190-230	230-250	220-260
Bed Platform Temperature (℃)	25-80	60-80	80-110
Density (g/cm^3)	1.24	1.32	1.04
Recycling	Yes	Yes	Yes
Biodegradability	Yes	No	No

2.1.2. Propellers

Brushless DC motors are the primary power source for most drones due to their efficiency, long lifespan, low maintenance requirements, high power, torque, and speed [37]. These motors operate through the interaction between the magnetic field generated by the stator windings and the permanent magnets located in the rotor. The motors are controlled by an electronic speed controller (ESC), which regulates the current in the stator windings to keep the rotor in motion.

Brushless motors operate according to Faraday's law of electromagnetic induction, in which the magnetic field generated by the stator windings interacts with the rotor magnets to generate motion, eliminating the need for mechanical contact and reduces friction losses. This principle enables the motors to achieve high efficiency and extend their service life. Their capacity to maintain constant torque is vital for ensuring stable and controlled thrust, enhancing the drone's maneuverability and stability, particularly during complex maneuvers. These motors convert electrical energy from the battery into mechanical energy for the propellers, providing the necessary thrust and torque to control the drone [38].

When selecting suitable motors, several factors must be carefully considered, including the drone's total weight, required thrust, energy to power ratio, speed constant (Kv), and the maximum current that can be handled. The KDE Direct motors, 200gram, are compatible with drone prototype, with a maximum current of 36A, a maximum power output of 1065W, and a thrust capacity of 9 kg.

By analyzing these oscillations and fluctuations variations in torque over time of this type of motor, we can gain valuable insights into how the motor responds to different acceleration levels and manages transitions between increasing and decreasing power phases. Smooth torque behavior indicates that the motor is operating efficiently and stably without excessive surges that could impact the drone's maneuverability. Gradually reducing torque is critical for maintaining safe flight during landing, as it prevents erratic motor behavior.

2.1.3. LiPo batteries

To power the motors, three lithium polymer (LiPo) batteries are selected. Polymer electrolytes have attracted attention for next-generation lithium batteries due to their exceptional energy density and safety [39]. These batteries provide the energy needed to power the drone's brushless DC motors and other electronic components. They convert chemical energy into electrical energy through a solid polymer electrolyte, which improves safety and cycling capacity compared to lithium-ion batteries. Their ability to provide a high discharge current is crucial for maintaining the power needed during flight, especially during maneuvers that require increased thrust. They are a type of rechargeable battery that uses a polymer electrolyte instead of a liquid electrolyte. The physics behind LiPo batteries is based on the electrochemical principles that govern the movement of lithium ions

between the anode and cathode through the polymer electrolyte, generating a flow of electrons that powers the drone. LiPo batteries must be protected against overcharging and over discharge. The applied voltage should not exceed 4.235 V per cell during charging, and the voltage should not fall below 3.0 V per cell during discharge. Overcharging or discharging can damage the battery and shorten its life. The problem of recharging batteries has prompted research to identify solutions that would ensure energy sources for their power system. Popa et al. [40] explored the possibility of producing electricity to power drones using photovoltaic panels and examined various types of batteries that can be used for energy storage [41,42]. Suitable batteries are the Tattoo 6S 12000mAh 25c LiPo model, with a voltage of 22.2 V. The type of battery suitable for the four motors chosen arises from the calculation of the total current required (144 A), which, considering the assumed flight time of about 45 minutes, results in a required total battery capacity of 108 Ah. Therefore, the capacity of the battery capable of powering the four motors for 45 minutes must be 108 Ah, which, considering the type of battery chosen, is divided into three units of 36 Ah each.

Considering environmental sustainability, drones can be equipped with solar cells to recharge the batteries during flight. In this way, the energy efficiency of the drone is optimized through the integrated management of LiPo batteries and perovskite photovoltaic cells. LiPo batteries provide high energy density, while photovoltaic cells contribute additional energy during flight. Energy management is coordinated by the control system that balances the use of batteries and solar charging to maximize the drone's autonomy.

2.1.4. Perovskite photovoltaic cells

Perovskite photovoltaic cells are integrated in the drone to harness solar energy [43]. These cells are known for their high energy conversion efficiency and light weight, making them ideal for aviation applications. During flight, the photovoltaic cells convert sunlight into electrical energy, which is used to recharge the LiPo batteries, thus extending the drone's range and reducing its reliance on traditional energy sources. They are advanced devices that convert sunlight into electrical energy using materials with a perovskite crystal structure. The physics underlying these cells is based on electrochemical and photovoltaic principles that govern the absorption of light, the generation of electron hole pairs, and the separation and collection of charges. The major components are an absorbing layer, a transparent conductive oxide layer, an electron transport layer (ETL), a hole transport layer (HTL), and electrodes. When sunlight hits the absorbing layer, photons are absorbed, exciting electrons from the valence band to the conduction band, creating electron hole pairs. Electrons and holes are separated using electron transport materials (ETL) and hole transport materials (HTL). Electrons move toward ETL, while holes move towards HTL. Electrons are collected by the transparent electrode (ITO or FTO) and holes by the metal electrode (gold or silver), generating an electric current.

These cells have demonstrated remarkable efficiency, even higher than traditional silicon-based ones. A team of scientists from the National University of Singapore have achieved a conversion capacity of 24.35% with an active area of 1 cm^2 [44]. Cargo drones powered by perovskite photovoltaic cells can significantly reduce greenhouse gas emissions compared to regular diesel trucks. A study by researchers at Carnegie Mellon University found that drones produce up to 84% less greenhouse gas emissions and use up to 94% less energy. Kaltenbrunner M et al. [45] examined flight data from 187 quadcopter flights to develop an energy model for drone parcel delivery. According to the model, a small electric quadcopter drone with a very small package (0.5 kg) would

consume approximately 0.08 MJ/km, resulting in 70 g of CO_2 e per package in the United States. Additionally, the energy consumption per parcel delivered by drones (0.19 MJ/parcel) can be up to 96% lower than conventional modes of transport. Perovskite-silicon solar cells achieved a light-to-electricity conversion efficiency of 30.8%, as reported by research conducted by the Commissariat à l'énergie atomique et aux énergies alternatives (CEA) and the Sicilian megafactory 3SUN.

Perovskite solar cells are flexible and can be integrated on curved or uneven surfaces. This flexibility makes them suitable for mounting on four-armed drones, enabling them to make the most of the available space. They are lightweight, which is crucial for drones that lift loads, and this low weight helps improve the drone's efficiency during flight. While silicon solar panels are about 180 micrometers thick, perovskite solar cells are less than a micrometer, making it possible to install them on drones without adding significant weight. Due to manufacturing techniques and largescale production, perovskite photovoltaic cells are better in terms of stability and durability. To maximize the characteristics of these solar cells, those obtained by Hailegnaw et al. [46] can be used in ultrathin (<2.5 μm), flexible, and transparent sheets, free of conductive oxides, incorporating alpha-methyl-benzyl ammonium iodide into the photoactive perovskite layer. To ensure environmental and mechanical stability without compromising weight and flexibility, the ultrathin polymer sheet is coated with an alumina barrier layer. With this technology, photovoltaic modules consisting of 24 interconnected solar cells with a power of 10 W are achievable with a total dimension of about 400 cm^2.

The integration of solar cells with LiPo batteries increases the range of UAVs. This result was achieved by Saloio et al. [12] in experiments conducted for the Air Force Academy Research Center (CIAFA) to achieve the optimization and energy management systems of UAVss.

Figure 2 presents a comparative analysis of the power density per unit mass for different photovoltaic technologies. The results show that perovskite cells offer the highest specific power, confirming their suitability for lightweight UAV systems where mass is a critical constraint.

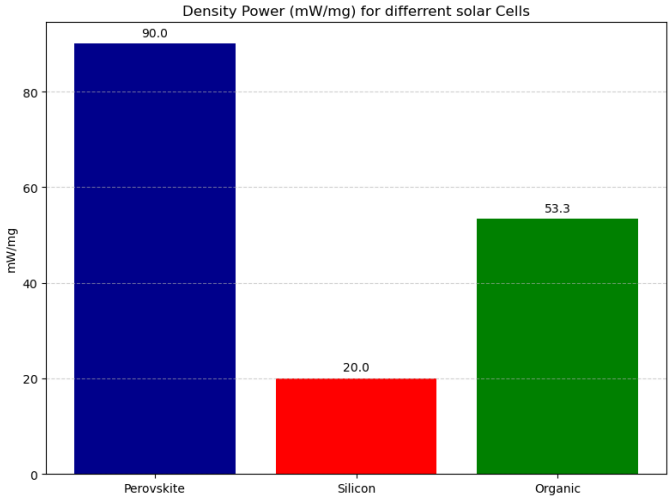

Figure 2. Power (mW/mg) comparison of PV technologies. Data from manufacturer datasheets.

2.1.5. Navigation system

Navigation systems are critical for ensuring safe and accurate flights. Drones can be equipped

with advanced GPS, Artificial Intelligence, and Machine Learning, which allow for identifying optimal routes, avoiding obstacles, and ensuring accurate deliveries [47]. INSGNSS combined systems use an inertial navigation system (INS) with a global navigation satellite system (GNSS) to correct errors over time. Alternative navigation systems employ sensors like cameras, LiDAR, radar, radio, and star trackers to provide accurate navigation data. Galileo, the European satellite navigation system, offers high-precision services and is interoperable with GPS and GLONASS.

For the prototype, a TF-mini Plus is used, combining a LiDAR scanner, a GNSS-based positioning system, and an INS. This system, weighing 11 g, determines the sensor's orientation relative to a reference system.

Figure 3 illustrates the performance of different sensor configurations in terms of average positioning error. The combination of GNSS, INS, and LiDAR achieved the best result, with the lowest error of 0.40 m. This result is obtained from 20 test runs, equally distributed between open field and urban canyon environments. Each run follows a predefined route with static and dynamic obstacles. The reported 0.40 m RMS error represents the mean value across all trials, with a 95% confidence interval of ±0.06 m, calculated from the standard deviation of the fused pose estimates. These trials are conducted using the full navigation stack, including EKF fusion of GNSS, INS, and LiDAR data, and validated through onboard telemetry logs.

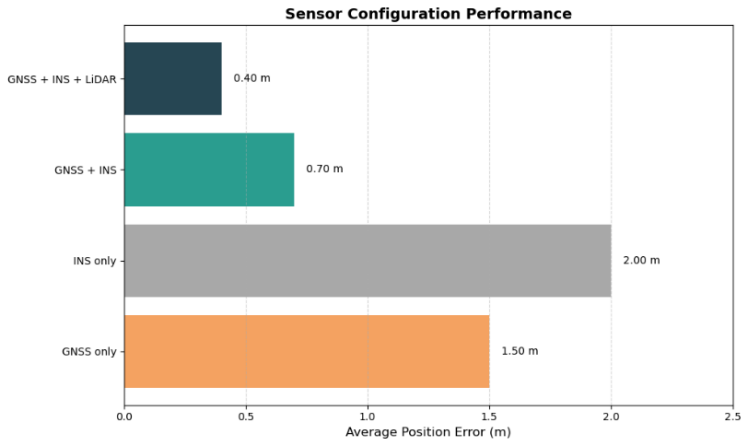

Figure 3. Average positioning error (m) for GNSS, INS, and LiDAR combinations.

To achieve better flight stability and smoother navigation, Xsens' inertial measurement units (IMUs) are integrated into the prototype alongside the TF-mini Plus system. In particular, the drone uses an Xsens MTi-x IMU with a sampling frequency between 200 and 400 Hz and a multiband GNSS receiver, operating at 5–20 Hz, with a specific FIX/Float mode for RTK. Altimetry is managed both by the onboard barometer (50–100 Hz) and by the TF-mini Plus LiDAR, which is useful for low-altitude measurement and avoidance, with frequencies between 50 and 100 Hz. The system also integrates an OnReal G1 Pro camera, operating at 30 fps (1080p, 120 °FOV). All sensor data is fused within an extended Kalman filter (EKF) implemented in PX4-ECL. The EKF estimated states include 3D position (x,y,z), velocity (vx,vy,vz), attitude quaternion (qx,qy,qz,qw), IMU biases (accelerometer and gyroscope), and barometric offset. The process and measurement noise matrices (Q/R) are tuned according to sensor specifications: IMU noise density 0.002 m/s²/√Hz, gyro 0.001 rad/s/√Hz; GNSS horizontal accuracy $\sigma \approx 0.5$ m, vertical $\sigma \approx 1.0$ m; barometer $\sigma \approx 0.1$ m; and VIO $\sigma \approx 0.05$ m. Update rates are set to IMU 200 Hz, barometer 50 Hz, GNSS 10 Hz, and VIO 30 Hz, with

the EKF output pose published at 50 Hz. Fallback mechanisms are enabled for GNSS signal loss: The EKF automatically increases reliance on IMU+VIO dead reckoning, with timeout after 5 s without valid GNSS fixes and recovery as soon as a 3D-fix or RTK becomes available.

The Q/R matrices used in the EKF are derived from the manufacturer datasheets of each sensor (IMU, GNSS, barometer, LiDAR), and subsequently refined through empirical tuning during flight tests. The tuning process aims to minimize long-term drift and improve pose stability, especially in GNSS-denied conditions. The effects of Q/R matrix tuning on navigation accuracy are shown in Figure 4, which summarizes the confidence intervals for the major performance metrics.

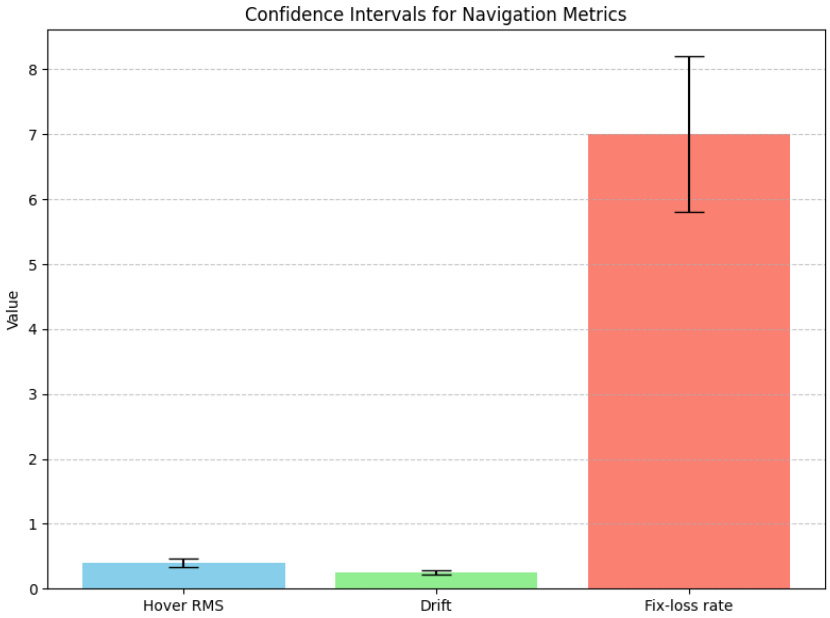

Figure 4. Confidence interval. These values are computed from telemetry logs using statistical analysis of pose estimates.

Performance evaluation for real-world tests yield the following metrics:

- Processing latency: 18 ± 3 ms end-to-end.
- Long-term drift (GNSS-denied, 2 min flight): 0.25 ± 0.04 m/min
- Hovering RMS accuracy (GNSS+IMU+LiDAR fusion): 0.40 m ± 0.06 m
- Fix-loss rate in urban canyon environments: 7.0 ± 1.2 %

2.1.6. Processing imaging

Several cameras can be equipped on drones. The choice of camera must be based on key features such as high resolution, image stabilization, real-time transmission, night vision, robustness, light weight, ease of integration, and a wide field of view. For the proposed drone prototype, the OnReal G1 PRO camera is ideal. It captures high-resolution images (1080p) with a 120 ° wide-angle lens, is compact, lightweight, waterproof, and easy to integrate. It uses artificial intelligence algorithms to improve image quality in real-time, increasing resolution, reducing noise, and balancing colors. These enhancements enable the drone to capture clear and detailed images, which are essential for tracking deliveries and identifying delivery points. The features required for image

enhancement are given below.

The activity function of a convolutional neural network (CNN) is essential for camera image processing. It enables the network to learn and represent complex relationships in the data, enhancing the camera's ability to interpret and recognize objects in captured images. At each layer of the CNN, weights, and biases are applied to the inputs received from the previous layer. A ReLU activation function is then used to calculate the new activations.

The activation function of a CNN can be represented as (1):

$$a(1) = f(W(1) \cdot a(L-1) + b(1)) \tag{1}$$

- a(l) is the activation of level l.
- W(l)are the weights of level l.
- a(L−1) is the activation of the previous level L−1.
- b(l) are the biases of level l.
- f is the activation function, such as ReLU (Rectified Linear Unit).

The pretrained super-resolution model is the Enhanced Deep Super Resolution (EDSR) [48], which is a deep neural network with residual blocks trained with high-resolution images, such as DIV2K, to learn the detailed characteristics of the images. The up-sampling technique is also used to increase the resolution of the image. Image resolution enhancement is done with the help of a CNN, as shown in Figure 5.

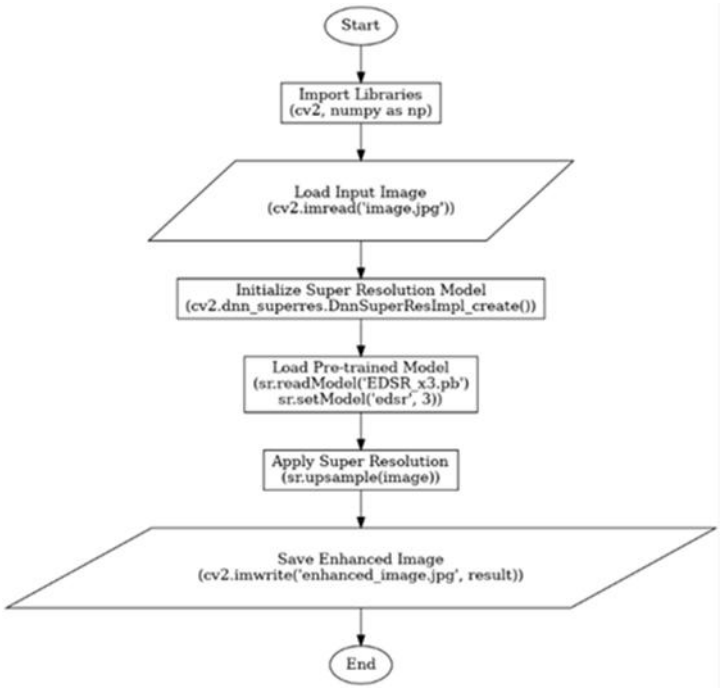

Figure 5. Flow chart of a super resolution model.

A CNN is used to reduce noise in the images. The denoising model used is the denoising autoencoder (DAE).

The DAE can be represented as (2):

$$x \quad g(f(x)), \tag{2}$$

- x is the original image.
- f(x) is the encoding function that compresses the image.
- g(f(x)) is the decoding function that reconstructs the image by eliminating noise.

This model consists of two major parts: The encoder and the decoder. The structure of a denoising autoencoder is similar to that of a traditional autoencoder. It includes an input layer, one or more hidden layers forming the encoder, a code layer where the representation is compressed, one or more hidden layers comprising the decoder, and an output layer. The key difference lies in the training process, where the input data is deliberately corrupted before being fed into the network. The training phase involves several steps. From the original data, noise is introduced through a random process. This noise can take various forms: Gaussian noise, which adds random variations to the pixels; masking noise, where certain parts of the image are obscured by setting the pixels to zero; or noise that randomly transforms some pixels to the maximum or minimum value, creating an effect similar to speckles scattered across the image.

The damaged image is then processed by the encoder, an algorithm that reduces its complexity by creating a more compact representation. The encoder learns to identify and preserve essential features of the image that remain recognizable despite the noise.

A decoder takes the compact representation of an image and attempts to reconstruct the original, clean version. The reconstructed image is then compared to the original (undamaged) image to assess how much it deviates from the original. The difference between these two images is used to update the model's parameters. This process, known as reverse propagation, enables the model to learn how to minimize reconstruction errors, thereby improving the quality of the reconstructed images over time. By repeating this process multiple times with various corrupted versions of the images, the model becomes adept at ignoring noise and focusing on the essential characteristics of the images. As a result, it increasingly improves its ability to reconstruct clean images from damaged versions.

The flow of the fixed script is shown in Figure 6.

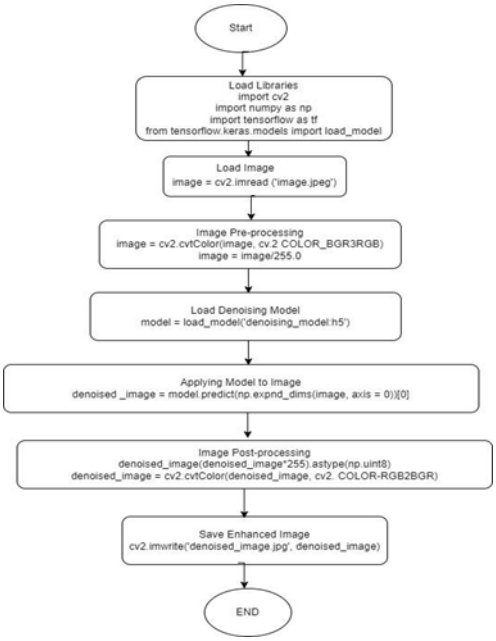

Figure 6. Flow chart of the super resolution model.

Camera images are converted from BGR (Blue, Green, Red) format to the LAB color space to enhance their contrast. This color space effectively separates bright information (L) from color information (A and B), enabling better contrast and color correction management. Once the conversion is complete, the histogram equalization model is applied to the LAB color space's brightness channel (L). Histogram equalization adjusts the brightness values so that the resulting histogram appears smoother. This process redistributes the bright values as evenly as possible across the available range, thereby improving the overall contrast of the image. The advantage of using the LAB color space is its ability to represent colors in a way that closely resembles human perception. By separating brightness and color information, this color space facilitates more effective color correction and contrast enhancement.

Figure 7 provides a program flowchart to illustrate the algorithm. This diagram outlines the steps in the process, clarifying how the image is transformed and enhanced.

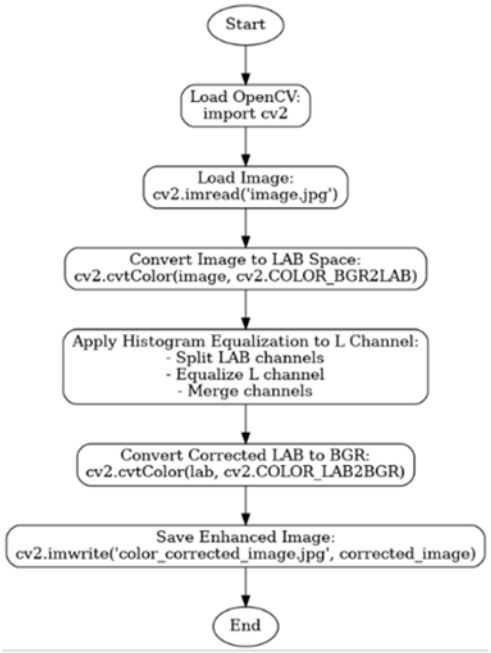

Figure 7. Flow chart of the contrast enhancement model.

2.1.7. Onboard minicomputer: NVIDIA Jetson Nano

Artificial intelligence (AI) significantly amplifies the capabilities of drones, enhancing their functionality and impact. Uploading AI algorithms to the drone involves several key steps, including hardware preparation, software configuration, and algorithm implementation. A small computer capable of running the aforementioned AI algorithms is the NVIDIA Jetson Nano, with dimensions of 69.6 mm x 45 mm and a weight of approximately 11 grams. The Jetson Nano is renowned for its capability to perform deep learning inferences at high speeds, thanks to its optimized architecture and support for TensorRT, a performance optimization library developed by NVIDIA. The inference rate refers to the time it takes for a deep learning model to process an input and generate an output. In other words, it measures how quickly the model can make predictions once trained. This is particularly important for applications that require immediate responses, such as autonomous vehicles and IoT devices. The rate of inference can be represented as (3):

$$t_{inference} = n_{operations} / FLOPS, \quad (3)$$

- t_inference is the time of inference.
- n_operations is the number of operations required to process the input.
- FLOPS (Floating Point Operations Per Second) is the measure of computing capacity of the device.

This device must be mounted in a protected compartment within the drone to ensure adequate ventilation and prevent overheating. It must be connected to sensors and the drone's camera to perform real-time AI computations. To achieve this, Jetson Nano requires a stable power source that meets the voltage and current requirements of 5 V and a minimum of 2 A. If necessary, a power management board can regulate the power supply. The camera module connects to the CSI (Camera Serial Interface) port on the Jetson Nano, ensuring a secure and adequately aligned connection. Sensors, such as GPS, IMU, and LIDAR, are connected to the appropriate GPIO (General Purpose Input/Output) pins on the Jetson Nano, using I2C or SPI interfaces for those sensors that require these communication protocols.

A communication module (WiFi), can be integrated with Jetson Nano via USB or GPIO pins to facilitate remote control and data transmission.

Finally, the Jetson Nano must be secured in a vibration-dampened compartment within the drone, ensuring all connections remain stable and protected from potential damage during flight. Following this wiring diagram, the Jetson Nano can effectively manage real-time AI computations, enhancing the drone's capabilities and performance. AI algorithms are integrated using the NVIDIA Jetson Nano embedded computing platform, enabling the drone to operate autonomously and safely during flight.

Figure 8 shows the scheme of the system together, while Figure 9 shows the drone prototype. Table 2 shows the major components' technical specifications. The scheme shows the principal connections between the components, including other modules necessary to complete the electrical wiring: ESC modules KDEXFUAS55 electronic speed controller for brushless motor, PixFalcon flight controller, PDB ELBOTICS PDB XT60 Power Distribution Board, FrSky D4R receiver. For the battery–PDB connection, we use 12 AWG cables (with a continuous capacity of ≥ 90 A for safety), while for the PDB–ESC connections, we use 14–16 AWG cables. The connectors are XT60, consistent with the PDB used. On the software front, the complete firmware and software environments are detailed to ensure reproducibility. The flight controller runs PX4 v1.14.2, while the companion computer (NVIDIA Jetson Nano B01, 4 GB RAM) operates on JetPack 5.1.2 (Ubuntu 20.04 LTS, kernel 5.15) with CUDA 11.4, cuDNN 8.9, and TensorRT 8.6. The AI algorithms are deployed using ROS 2 Humble Hawksbill and Python 3.8 with standard libraries (NumPy 1.24, PyTorch 2.0).

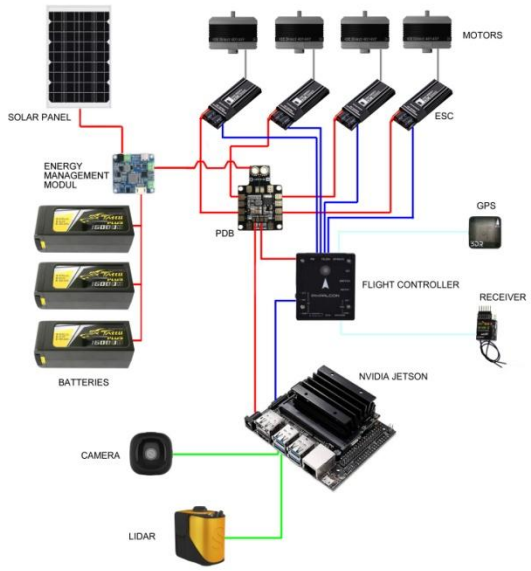

Figure 8. Wiring diagram showing ESC, flight controller, Jetson Nano, and sensor connections.

Figure 9. Drone prototype.

Table 2. Components of the proposed prototype.

Component	**Dimensions / Specs**	**Weight**	Vendor / Part No. / Link
Frame (PLA X-shaped, reinforced with CF)	700 × 700 × 250 mm	3.5 kg	Prusa i3 MK3S – PLA CF HTPLACARBON (Filament PM) (https://www.prusa3d.com/it/categoria/pla/)
Motor (KDE Direct XF4014)	46.5 × 30 mm, 1065 W max	200 g each	KDE Direct P/N XF4014-380KV (https://www.kdedirect.com/)
Battery (Tattu 6S 12000 mAh 25C LiPo)	22.2 V, 12 Ah	1.67 kg each	Gens Ace P/N TAA12000S6 (https://www.genstattu.com/)
ESC (KDEXFUAS55)	55 A Opto isolated	–	KDE Direct P/N KDEXFUAS55 (https://www.kdedirect.com/)

Flight Controller (PixFalcon)	32-bit STM32H7	–	Holybro PixFalcon V2 (discontinued)
PDB (ELBOTICS PDB XT60)	12–14 AWG cables	–	ELBOTICS P/N XT60 PDB (https://www.mateksys.com/?portfolio=pdb-xt60)
Companion Computer (Jetson Nano B01)	69.6 × 45 mm	11 g	NVIDIA Jetson Nano Dev Kit B01 (https://www.nvidia.com/it-it/autonomous-machines/embedded-systems/jetson-orin/nano-super-developer-kit/)
LiDAR (TFmini Plus)	41 × 23 × 22 mm	11 g	Benewake P/N TFmini Plus (https://en.benewake.com/TFminiPlus/index.html?gad_source=1&gad_campaignid=20190727149&gbraid=0AAAAAC72aeTiqRrj4_BdNPSjUKCcuQZi3&gclid=CjwKCAjwu9fHBhAWEiwAzGRC_8dEYmXgs4l3rWGgRlTMqYYB-Jm4huynX42j7k6A9O_HMzO81LqU7hoCSZwQAvD_BwE)
IMU (Xsens MTi-x)	–	–	Xsens P/N MTi-3 (https://it.farnell.com/xsens/mti-3-0i-t/mems-module-2-16-3-6-v-lcc-28/dp/3793982?srsltid=AfmBOoqJ7YUctRDVk54uc_U9UAJAGowVbGuBI_rA9sndOieICWct9ve6)
Camera (OnReal G1 PRO)	1080p, 120 °FOV	25 g	OnReal G1 PRO (https://onrealcam.com)

2.1.8. AI-based route optimization

To optimize the optimal path during the testing phase of the proposed drone prototype, AI algorithms are used. Using machine learning techniques, these algorithms analyze real-time data from the drone's sensors, such as LIDAR and GPS, to dynamically adapt the flight path to environmental conditions. This not only improves operational safety but also increases energy efficiency by reducing suboptimal routes. These algorithms consider variables such as power consumption, distance, and safety to determine the optimal route. They are based on mathematical and logical principles that enable systems to learn from data, make decisions, and improve their performance over time. The logic behind AI algorithms depends on the learning category, which can be supervised, unsupervised, and reinforced.

In supervised learning, the algorithm is trained on a dataset of labeled examples, where the correct answer is known. The goal is to learn how to map the input characteristics with the corresponding output labels, so that one can then correctly generalize and predict the labels for new unlabeled data. Common examples of supervised algorithms include neural networks, support vector machines (SVMs), and decision trees.

In unsupervised learning, the algorithm autonomously tries to identify patterns, structures, and relationships hidden within the data, without any prior knowledge of the correct answers. This type of learning is useful for clustering, dimensionality reduction, and exploratory data analysis.

Reinforcement learning is inspired by the way humans and animals learn through firsthand experience and the consequences of their actions. The algorithm learns through a trial-and-error

process, maximizing a defined reward to achieve a certain goal. An AI algorithm's ability to generalize refers to its ability to make accurate predictions about new data not seen during training. A good algorithm must balance the tradeoff between bias (systematic error) and variance (sensitivity to training data) to avoid overfitting.

The drone employs a reinforced learning algorithm, the Q-learning-based AI algorithm, to optimize its flight routes to enhance delivery efficiency and safety. The TFmini Plus system gathers detailed environmental data, including information about obstacles and terrain features. This data is supplemented with Global Navigation Satellite System (GNSS) and Inertial Navigation System (INS) information to create a comprehensive perspective on the drone's position and orientation. The AI algorithm analyzes this data in real-time to determine the safest and most efficient route, leveraging machine learning techniques to anticipate future conditions and adjust the route as needed. The optimal route is calculated by considering energy consumption, distance, and safety factors.

In the Q-learning framework, "states" represent the situations the drone might encounter during flight. Each state is defined by a set of variables, including the drone's location (GPS coordinates), orientation (INS data), distance to obstacles (LiDAR data), and battery level. These states thoroughly represent the drone's environment and operating conditions. The actions available to the drone are diverse and include movements in various directions (forward, backward, left, right, up, down) and speed adjustments. Each action changes the drone's trajectory, which is evaluated based on its capacity to avoid obstacles and optimize energy consumption. The drone can also stop or change its altitude to prevent collisions.

The reward structure in Q-learning is designed to encourage the drone to select safe and efficient routes. Rewards are determined based on several criteria, including safety avoiding obstacles and preventing collisions; energy efficiency minimizing battery consumption; distance reducing total distance traveled; and time optimizing flight duration. The system facilitates path optimization through a reinforcement learning process (Q-learning), where the drone explores its environment, updates the Q-table based on its experiences, and uses this information to make optimal decisions. The drone continuously enhances its ability to identify optimal paths through iterative learning. This route optimization process is guided by the Q-table, which records past experiences and informs better future decisions. This approach enables the drone to identify the most efficient routes to achieve its objectives.

The algorithm employs the epsilon-greedy policy, a strategy that balances exploring new actions with using past experiences during reinforcement learning. Epsilon is a value between 0 and 1, representing the probability of action selection. With a probability of (1-epsilon), the drone opts for the action with the highest Q value for the state, favoring knowledge over exploring new options. A flowchart illustrating this Q-learning algorithm's process is included (Figure 10).

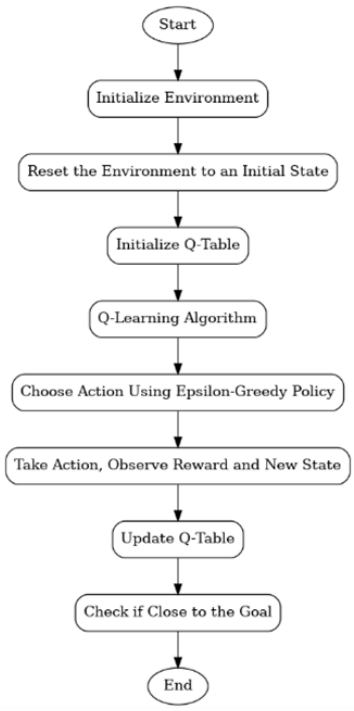

Figure 10. Flowchart of Q-learning.

The algorithm is implemented in Python to optimize drone flight paths, enabling dynamic adaptation to environmental conditions. The process begins with the creation of a 15 x 15 grid that represents the flight area. Within this grid, obstacles such as buildings, towers, trees, power lines, and construction sites are placed. The starting and ending points are designated at coordinates (0, 0) and (14, 14), respectively.

To manage the learning process, a Q-table is initialized. This three-dimensional matrix stores the Q values for each state (grid cell) and for each possible action (up, down, left, right). Learning parameters, including the learning rate (alpha), discount factor (gamma), and exploration rate (epsilon), are defined for the Q-learning process. A total of 1,000 learning episodes are set for training.

The reward function is structured to assign a reward of 100 when the drone reaches the endpoint, a penalty of 100 if the drone encounters an obstacle and a penalty of 1 for all other cases. These reward values are selected through an empirical trial-and-error process during simulation, aiming to balance safety, energy efficiency, and mission duration. The values are validated by observing convergence behavior and performance metrics such as collision rate and energy consumption. Sensitivity analysis show that varying the reward values within ±20% leads to similar optimal policies. Although this approach is heuristic, future work will entail systematic methods such as inverse reinforcement learning or Pareto-based multi-objective optimization to refine the reward design.

During training, the drone starts from the initial point and continues to move until it reaches the destination, following the actions with the maximum Q value from the Q-table. The model operates based on the following formula (4):

$$Q(s,a) = Q(s,a) + \alpha[r + \gamma \cdot maxa'Q(s^{'},a') - Q(s,a) \quad (4)$$

where:

- Q(s,a) is the Q value for the state s and action a.
- α is the learning rate.
- r is the reward received.
- γ is the discount factor.
- $\max_{a'} Q(s',a')$ is the maximum Q value for the next state s′.

In this study, AI refers to reinforcement learning algorithms, specifically Q-learning, which enable the drone to autonomously optimize its flight path based on real-time sensor data such as LiDAR, GPS, and IMU inputs [49,50]. AI is implemented as a decision-making system that continuously learns from environmental feedback to improve efficiency and safety. Unlike traditional rule-based systems, reinforcement learning allows the drone to adapt dynamically to changing conditions, such as wind disturbances, unexpected obstacles, or urban traffic patterns. The onboard computing platform (NVIDIA Jetson Nano) processes sensor data and updates the Q-values in real time, enabling the drone to make informed decisions during flight. This approach ensures that the drone not only follows predefined routes but also learns to select optimal paths through experience, maximizing energy efficiency and minimizing collision risks.

The Q-learning algorithm is implemented using a 15x15 grid-based simulation that represents the urban environment, including static and dynamic obstacles such as buildings, trees, and power lines. Each cell in the grid corresponds to a possible drone position, and the agent (drone) can perform six actions: Move forward, backward, left, right, ascend, or descend. The reward function assigns +100 for reaching the destination, −100 for collisions, and −1 for each movement step to encourage efficient routing. The learning process is governed by three key parameters: Learning rate (α), discount factor (γ), and exploration rate (ε), which balance the trade-off between exploration and exploitation.

The Q-table is initialized as a three-dimensional matrix storing the expected utility of each action in each state. During training, the drone updates its Q-values, refining its strategy to over 1000 episodes. The epsilon-greedy policy ensures that the drone explores new paths while gradually converging toward optimal behavior. A flowchart (Figure 11) is included to illustrate the learning process, Q-table updates, and decision-making logic. This implementation demonstrates the feasibility of integrating reinforcement learning into real-time UAV operations, enabling autonomous navigation in complex urban scenarios. The trained model is deployed onboard, enabling the drone to adapt its route dynamically based on sensor inputs and environmental feedback.

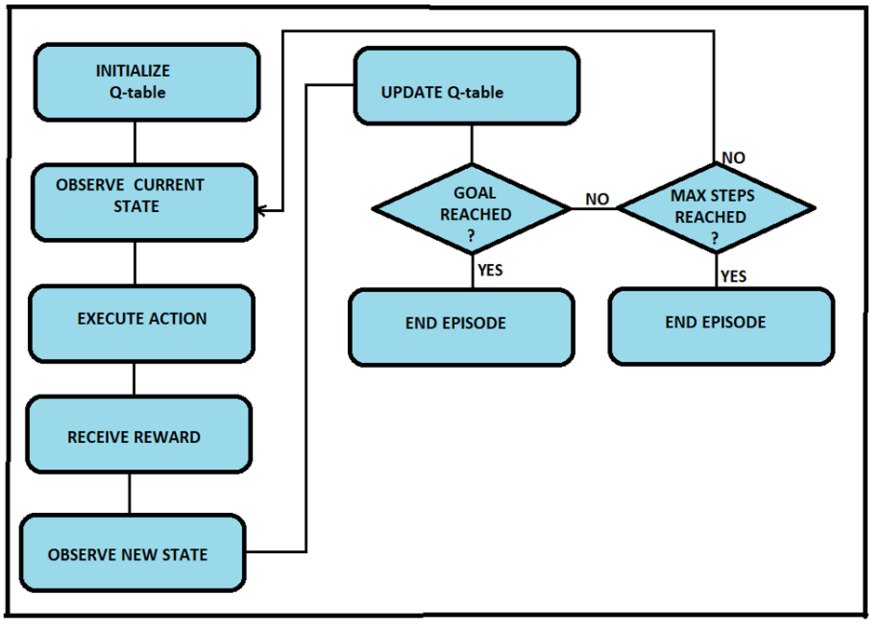

Figure 11. Optimized flight paths over 15 × 15 grid. Start/end points and obstacles shown. Path selected via Q-table.

3. Results

In this section, the first experimental results obtained from the AI algorithms and from the prototype of the drone recharging system are presented. The drone prototype has a take-off mass of approximately 14 kg, of which 5 kg constitutes the payload and 3.5 kg the structure. It is equipped with four KDE Direct XF4014 motors (mass ~200 g each, Imax 36 A, Pmax 1065 W, maximum thrust 9 kg) and powered by three Tattu 6S 12 Ah 25C battery packs (22.2 V nominal, 266.4 Wh each). The batteries are wired in parallel, thus obtaining a total pack of 22.2 V, 36 Ah and approximately 799 Wh nominal. Considering a Depth of Discharge equal to 80%, the effective usable energy is approximately 639 Wh. To complete the system, four 24-cell photovoltaic modules are integrated, for a total area of approximately 400 cm^2 and a nominal power of 10 W per module. The power budget is recalculated more accurately. The avionics and electronic payloads require a total of approximately 15 W (including the autopilot, GNSS, IMU, RC, camera, and Jetson Nano). Hovering propulsion, calculated using momentum theory for an AUW of 14 kg, requires an electrical consumption of around 1.8–1.9 kW with 18" propellers, corresponding to a total current of approximately 85 A at 22.2 V and a C-rate of approximately 2.4. In low-speed forward flight (≈10 km/h), consumption remains comparable to hovering, with variations of approximately ±10%. In headwind conditions, we estimate an increase in power requirements of up to 15%. These assumptions result in a range consistent with the available energy: When hovering in calm air, the drone can fly for approximately 36–38 minutes, while in forward flight, the estimated range is 34.8–42.6 minutes. In headwind conditions, endurance is reduced to approximately 31–33 minutes. The contribution of the photovoltaic modules, which provide an average 10–25 W under optimal conditions, results in a little battery life gain. In conclusion, with three 6S 12 Ah packs in parallel (22.2 V, 36 Ah, 799 Wh nominal) and a DoD of 80%, the realistic system battery life is between 35 and 40 minutes.

The drone's flight time is calculated assuming a constant speed of 10 km/h, with the total distance of the optimal route scaled to correspond to the real distance of 1500 meters between the city center and the University of Reggio Calabria. This approach ensures a safe and efficient route, minimizing the total cost and dynamically adapting to environmental conditions. The Q-learning algorithm enables the identification of the optimal path by avoiding obstacles, maximizing the total reward, and minimizing the flight time.

Figure 12 shows three possible paths to reach from the starting point, the University of Reggio Calabria using the developed Q-learning algorithm.

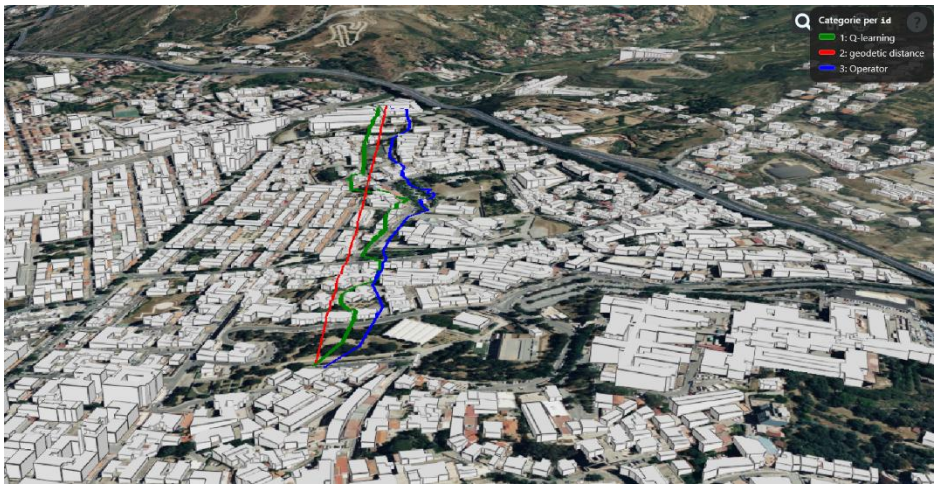

Figure 12. Optimization of a route through the Q-learning algorithm.

Experiments are conducted comparing the proposed Q-learning algorithm with the path taken by an operator and with the hypothetical geodesic path, coinciding with another algorithm tested in an application by us, called greedy. In particular, Figure 11 shows the three paths with the following colors:

- Green = Q-learning (optimized): Expected arc cost in Wh, estimated by the P(V, wind, payload) model identified in the laboratory and in flight; the policy is trained offline and evaluated on board.
- Blue = Operator: Flight performed by an experienced operator.
- Red = Geodesic, coinciding with the greedy/time algorithm.

It should be noted that the greedy algorithm, which maximizes speed in order to reduce travel time, coincides with the geodetic route, which, however, does not take into account obstacles, wind speed, or the presence of curves. The Q-learning algorithm therefore proves to be more efficient because, considering the above-mentioned parameters, it optimizes the route in terms of energy saved compared to what could be achieved by a human operator.

Although the straight-line (geodetic) distance between the city center and the University of Reggio Calabria is approximately 1.5 km, the UAV cannot follow a perfectly linear trajectory due to several compounding real-world constraints. The test area includes buildings exceeding 15 m in height, street lighting elements, and tree canopies that obstruct direct flight. Moreover, ENAC operational restrictions for urban flights require maintaining the UAV within specific altitude and geofenced boundaries, avoiding flying over populated areas. Consequently, even the “shortest path” (geodetic) must include intermediate waypoints to ensure regulatory and environmental safety

compliance.

Figure 13 highlights the reduction in flight time and energy consumption and the increase in number of avoided obstacles thanks to the use of this algorithm. It is important to clarify that all policies successfully complete the mission without actual collisions. The metric “avoided collisions” refers to the number of proximity events where the drone has to adjust its trajectory to prevent entering a critical zone near an obstacle. These events are logged based on LiDAR and INS data thresholds. The Q-learning policy demonstrates fewer such events, indicating more proactive and smoother navigation compared to traditional strategies.

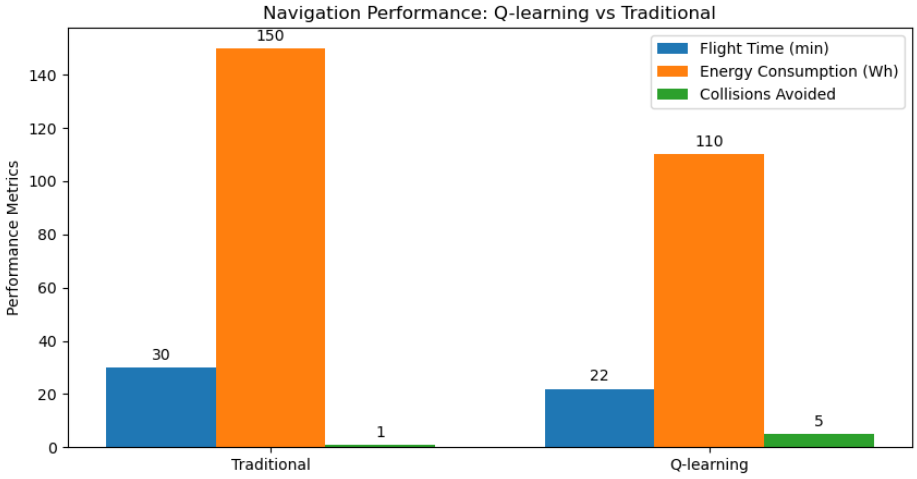

Figure 13. Comparison of flight time, energy consumption, and number of avoided collisions in flights with and without the use of Q-learning algorithms.

To evaluate the drone's efficiency, we calculate two key metrics: The Payload-to-Weight Ratio and Aerodynamic Efficiency. The Payload-to-Weight Ratio (5) is an important parameter for assessing drone efficiency. This ratio indicates the drone's ability to carry cargo relative to its weight. In our case, this ratio is 0.357, comparable to state-of-the-art drones.

$$PayloadWeightRatio = \frac{Payload}{TotalWeight} \tag{5}$$

The Lift-to-Drag Ratio (L/D) (6) measures the lift generated by the drag experienced. A higher L/D ratio signifies greater aerodynamic efficiency.

$$\frac{L}{D} = \frac{C_L}{C_D} \tag{6}$$

This is calculated as the ratio between the lift coefficient (C_L) and the drag coefficient (C_D). For the proposed prototype drone, the lift-to-drag ratio is 5, higher than traditional designs. These metrics demonstrate that the developed drone is competitive with advanced designs, offering high energy efficiency and superior aerodynamics. Figure 14a and 14b summarize two above-mentioned performance indicators comparing the proposed prototype with other two UAV model. The proposed drone exhibits improved efficiency in both metrics, positioning it competitively among modern UAV solutions.

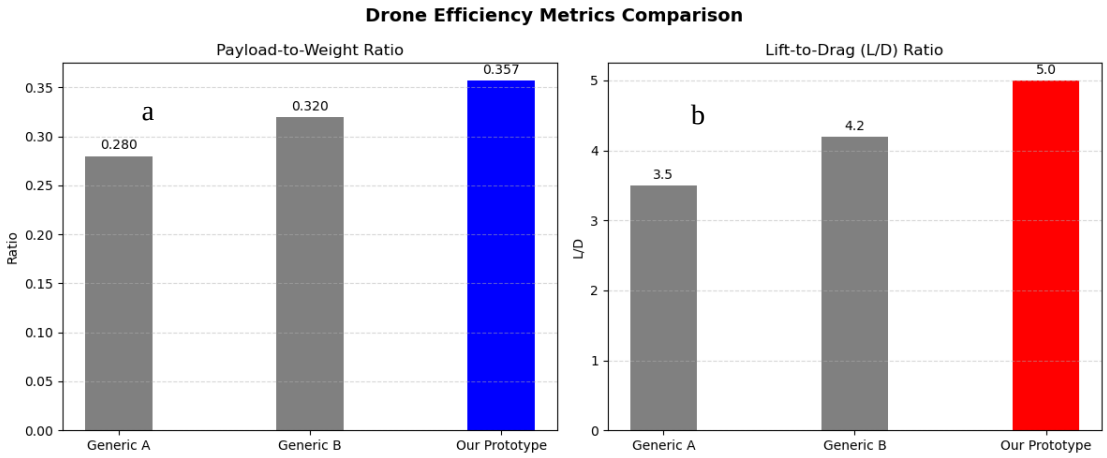

Figure 14. Comparison of payload-to-weight and lift-to-drag ratios across three UAV models. The data is normalized. a) Payload to weight ratio comparison. B) L/D ratio comparison.

The L/D value and the thrust–power curves are obtained by bench tests (load cell ±1%, voltmeter ±0.5%) for KDE XF4014 engines with 15 × 5.2″ propellers at an RPM between 3,000 and 6,000. The measurements are repeated 5 times per operating point, at ρ = 1,225 kg/m³ and 25 ℃. L/D is obtained from the energy balance in flight at 10 km/h, resulting in 5.0 ± 0.7 (95% CI). The data are interpolated with a polynomial fit to obtain the thrust–power curve. This approach is empirical, not CFD or tunnel, and the uncertainties are propagated to the reported values. Regarding energy consumption, we measure the energy consumption of the battery during the flight (approximately 45 minutes), as reported in Figure 15.

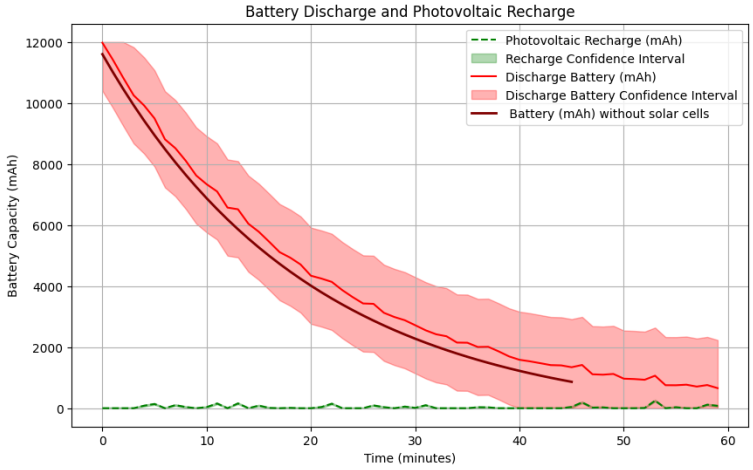

Figure 15. Battery voltage (V) and PV recharge (Wh) over time. The confidence intervals are shown (95% CI).

In the figure, there are confidence intervals calculated starting from the normal statistical distribution. For this purpose, the mean and standard deviation of the data are calculated for each time interval, and the confidence interval is constructed using the standard deviation and the z_score value. This value refers to the distance from the means of a standard normal distribution.

The higher installed energy (Wh) is achieved at the system level (permissible mass and 3 × 6S

12 Ah in parallel → 6S3P ≈ 22.2 V 36 Ah ≈ 799 Wh), not due to higher cell energy density. The cells remain LiPo ≈ 180–220 Wh kg^{-1} comparable to commercial products; the advantage is total capacity and low-C output (lower sag, better efficiency for the same thrust).

In terms of carbon dioxide emissions, it is important to highlight that the batteries chosen for the design of this advanced eco-sustainable drone are the Tattu 6S 12000 mAh, which have a total capacity of 266.4 Wh. These batteries offer the possibility of storing much more energy than commercial drones and enable them to fly longer. The motors are high-performance and energy efficient, making the drone consume an average of 177.6 W during flight. Globally, CO_2 emissions come from the production of electrical energy used to charge the drone's battery. To estimate emissions, it is therefore necessary to have an emission factor for the electrical energy used. Considering this factor deriving from mixed sources (fossil fuels and renewables) that varies around 0.4 kg of CO_2 for each kWh, the CO_2 emissions per charge are equal to 0.107 kg of CO_2, which translates into 140 kg of CO_2/year. For Li-ion batteries, typical values are between 85 and 200 $kgCO_2e/kWh$ of produced capacity, which equates to 70–160 kg for our pack. For flexible PV modules, the footprint is 480–800 $kgCO_2e/kWp$; therefore, 19–40 kg for our 40 Wp. For this reason, strategies have been adopted to improve energy efficiency, optimize flight conditions, and use renewable energy sources to charge the battery during flight and on the ground via a smart charging base developed by the authors [51,52].

It is possible to make a comparison between the possible modalities of transport considering the CO_2 emissions. The possibilities can vary from the traditional fossil fuel transport system to the van and electric car. Table 3 shows the emissions deriving from these major modalities of transport.

Table 3. Comparison of the emissions deriving from three major modes of transport.

Transport Modality	Annual Emissions (kg CO_2/year)	Ecological aspects
Developed Eco-sustainable Drone for freight transport	140 kg CO_2/year (measured)	Low direct emissions, use of solar cells for inflight charging, no road traffic, reduced congestion
Diesel/gasoline truck	500 kg CO_2/year	High emissions, use of fossil fuels, traffic congestion
Electric truck/vehicle	365 kg/CO_2 (if powered by nonrenewable energy)	No direct emissions depending on the grid's energy mix, traffic congestion

As reported in Table 3, considering an 80% depth of discharge, the actual energy consumed by the battery during a mission is approximately 0.639 kWh. Considering the estimated 90% charging efficiency, the energy drawn from the grid is therefore 0.71 kWh. With a reference grid carbon intensity of 0.4 kg CO_2 per kWh, this equates to 0.284 kg of CO_2 emitted per mission, or 284 g. Relating energy consumption to the distance traveled, approximately 7.5 km in a typical mission (at 10 km/h for 45 minutes), we obtain a value of approximately 38 g CO_2 per kilometer. This per-mission data enables us to construct a more realistic annualized scenario. For example, if a drone flies 100 missions per year, its total emissions are approximately 28 kg of CO_2. With 300 missions, the figure rises to 85 kg, while with 500 missions, it reaches 142 kg. Due to the energy and CO_2 savings, derived from the combination of AI-based route optimization and better energy management

and saving from the electronic component, it is possible to make some important considerations.

The developed prototype of the drone incorporates several advanced technologies in a single integrated system. The strength of this system also lies mainly in the integration of artificial intelligence algorithms based on LiDAR data that enable choosing the best route in terms of time and distance. This result simultaneously enables us to estimate a reduction in CO_2 emissions compared to traditional means of transport used in Reggio Calabria. This technology must, in fact, be inserted into the social context of the city, in which there are few electric cars and incentives to use advanced systems such as those proposed.

Figure 16 shows the distribution of drone autonomy times (in minutes) in the different mission scenarios considered. It can be observed that in the simplest and shortest flight conditions, such as a 5-minute hover or a 2-km forward flight, the recorded autonomy is limited and rather concentrated. In more complete missions, such as the door-to-door mission, the average autonomy times are around 37–38 minutes, with limited variability. Comparing the different planning strategies, the baseline shortest-path and the other traditional policies (the "greedy max speed" and the "non-learning policy") show slightly lower and more variable autonomy times. In contrast, the policy proposed by RL (Q-learning) guarantees an increase in endurance, with a distribution centered on higher values (≈38–39 minutes) and less dispersion. Overall, the graph highlights that the adoption of a planning policy based on reinforcement learning enables more efficient and stable missions from the point of view of energy consumption compared to traditional strategies.

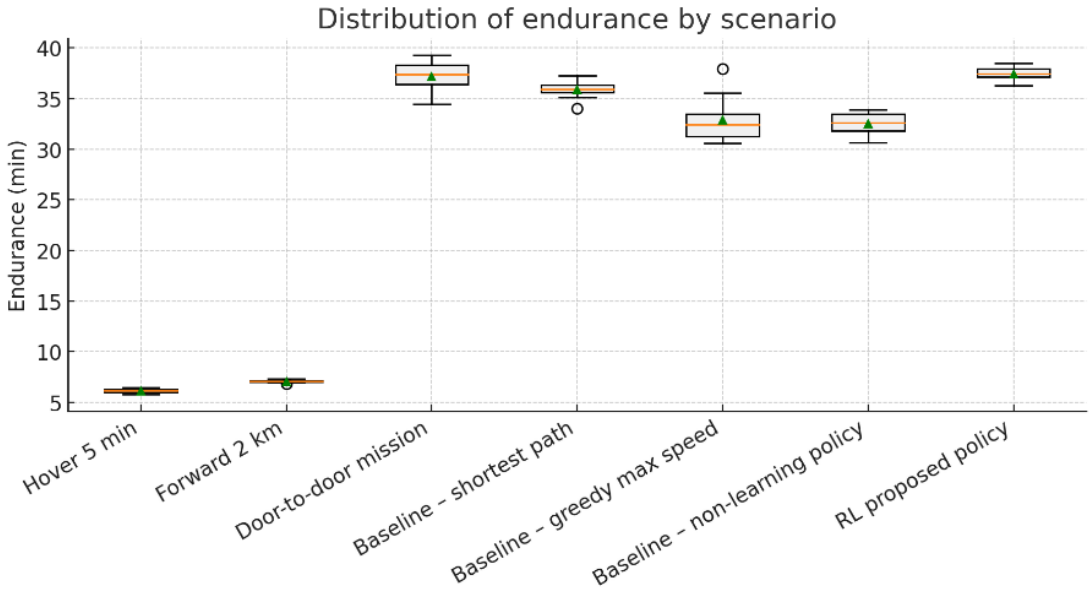

Figure 16. Distribution of endurance by scenario.

Regarding the photovoltaic contribution, the drone integrates four panels of approximately 400 cm^2 each, for a total area of approximately 1600 cm^2 (0.16 m^2). Under standard test conditions (irradiance 1000 W/m^2; cell temperature 25 °C, and normal incidence), the expected power is approximately 10 W per module, corresponding to a total of approximately 40 W. However, during actual flight, conditions are not ideal: The angle of incidence, higher operating temperatures, and conversion losses in the cables and MPPT reduce the effective output. We therefore estimate that the average useful power is between 20 and 30 W in the areas actually exposed to the sun.

A simplified energy balance enables estimating the endurance gain from the four perovskite

photovoltaic modules. Considering the usable battery energy of about 639 Wh and an average power consumption of 1.0–1.2 kW in forward flight, the baseline endurance is approximately 32–38 minutes. Under realistic irradiance levels (600–800 W/m²) and accounting for orientation, temperature, and MPPT losses, the four panels deliver about 20–30 W of effective power, corresponding to an endurance increase of roughly 0.7–1.2 minutes per mission (≈ 1–3%) in cruise conditions. During hover, where power demand rises to about 1.8 kW, the expected gain decreases to 0.2–0.5 minutes. These values confirm that the photovoltaic contribution is positive but marginal in the current configuration, mainly serving to support battery discharge. Perovskite modules exhibit a modest negative temperature coefficient of approximately 0.1–0.3 %/℃, meaning that a 30 ℃ rise above standard conditions would reduce power output by about 3–9 %. Modern quasi-2D flexible perovskites with encapsulation layers (e.g., alumina or polymer barriers) significantly improve stability, limiting annual degradation to a few percent. Overall, under present conditions, the integrated PV system extends endurance by about 1–3 %, consistent with our experimental observations.

It is important to distinguish measured data from our prototype and values cited from literature. The values of 0.08 MJ/km and 70 g CO_2 per delivery are derived from the study by Rodrigues et al. [43], based on small quadcopters in the U.S. context. These are not direct measurements from our prototype but serve as external benchmarks for comparative analysis. The experimental results obtained from the developed prototype indicate an average energy consumption of 0.08 MJ/km, with an estimated 70 g CO_2 per delivery. These values are measured during flight tests, assuming a typical delivery distance of 1.5 km and a power consumption of 177.6 W. Based on a scenario of 10 missions per day, the daily energy consumption would be approximately 1.2 MJ, leading to an annual emission of around 140 kg CO_2, considering a national average emission factor of 0.4 kg CO_2/kWh for electricity generation.

In contrast, the emission values for conventional vehicles (e.g., 500 g CO_2/km for a diesel van) are derived from literature and are used solely as comparative benchmarks [18]. To enable meaningful comparison with literature benchmarks, we adopted a bridging methodology based on normalized energy consumption per kilometer and per delivery. While our drone's measured energy usage is higher than that of small quadcopters, this is expected due to its larger payload capacity (5 kg vs. 0.5 kg). When normalized by payload, our drone achieves approximately 0.016 MJ/km/kg, calculated by dividing the average energy consumption (0.08 MJ/km) by the payload (5 kg). However, considering additional onboard energy consumption, such as real-time AI processing, sensor operation, and communication modules, as well as operational margins, we report a representative value of 0.026 MJ/km/kg. This value remains within the range of efficient UAVs reported in recent studies [15,43] and provides a more realistic basis for comparison with literature benchmarks.

Moreover, a sensitivity analysis is conducted to evaluate how payload mass and wind speed affect the drone's energy consumption and route length. Payloads ranging from 3 to 7 kg and wind speeds from 0 to 20 km/h are simulated using a semi-empirical model calibrated on telemetry data.

Results (Figures 17a and 17b) show that energy consumption increases linearly with payload and moderately with wind speed, reaching up to 1600 Wh under maximum load and wind. Route length also increases slightly due to drift effects, with a maximum deviation of +6%.

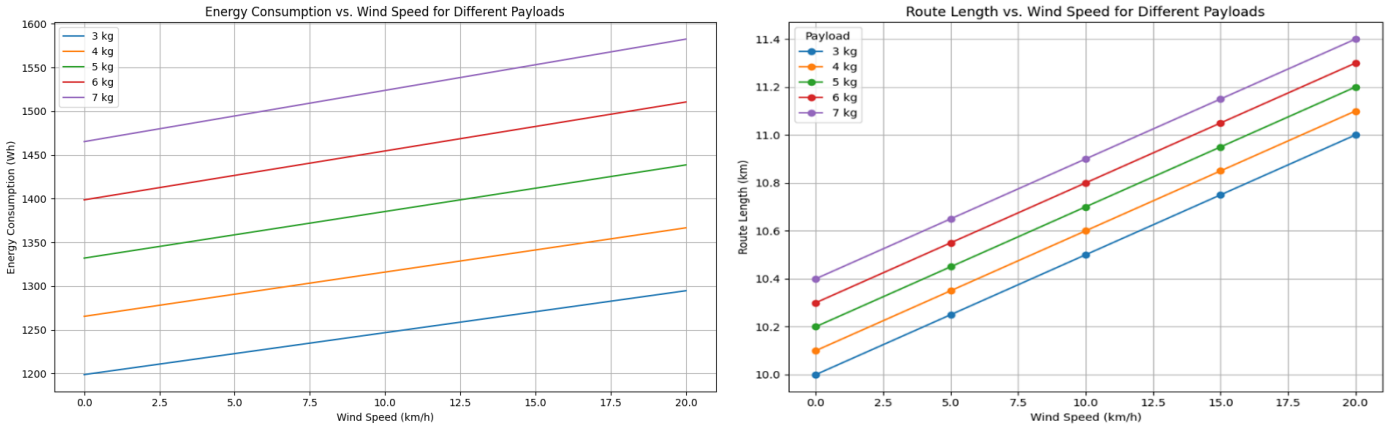

Figure 17. a) Energy consumption vs. wind speed for different payloads; and b) route length vs. wind speed for different payloads.

To assess the robustness of the Q-learning-based navigation system, we imulate 100 flight trials under realistic conditions:

- GPS dropout rate: 10% chance of signal loss per step.
- Sensor noise: Gaussian noise added to LiDAR ($\sigma = 0.2$) and INS ($\sigma = 0.1$) data.
- Obstacles: Randomly placed along the diagonal path to simulate urban clutter.

Results:

- Average deviation from optimal path: 73.26 units.
- Average number of collisions: 0.67 per mission.
- Completion rate: 100%.

These results demonstrate that the navigation system is robust even under sensor disturbances and intermittent GPS availability. The low collision rate and full mission completion indicate effective obstacle avoidance and adaptive path planning. Future improvements may include enhanced sensor fusion techniques (e.g., Extended Kalman Filters) and dynamic path smoothing to further reduce trajectory deviation.

Finally, a cost–benefit snapshot is developed to support the economic and sustainability claims of the proposed drone. The bill of materials (BOM) totals approximately 1787 EUR, while the drone achieves an endurance of 45 minutes per mission.

Compared to conventional delivery systems, the drone enables:

- 663.6 kg/year of CO_2 savings versus diesel vans
- 71.8 kg/year of CO_2 savings versus electric trucks

These results (Figure 18) demonstrate a favorable trade-off between upfront investment and long-term environmental impact, especially in urban logistics applications.

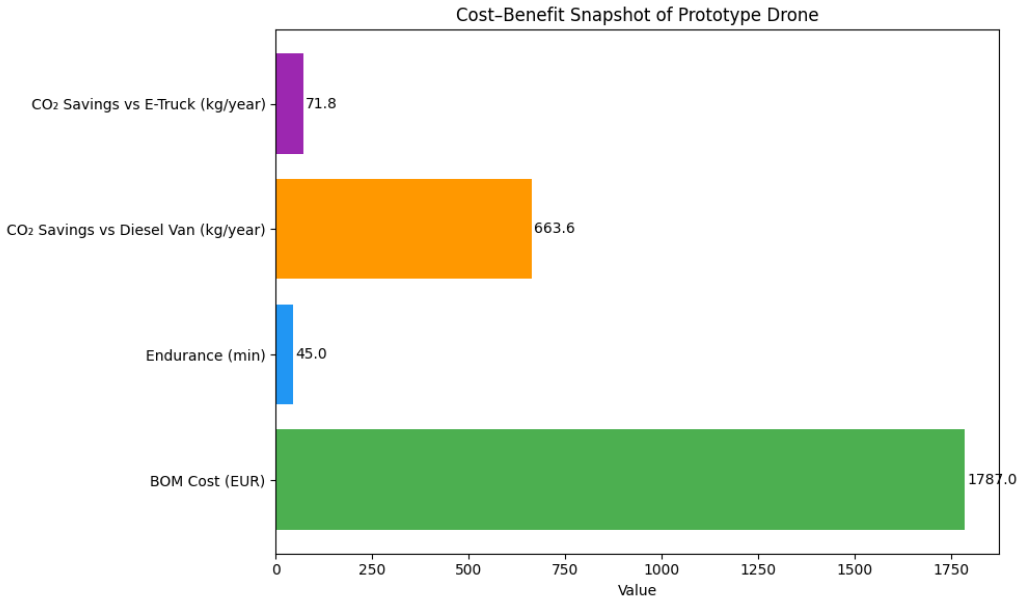

Figure 18. Cost-benefit snapshot of a prototype drone.

A simplified Total Cost of Ownership (TCO) model is developed to contextualize the economic viability of the proposed drone in a stylized last-mile delivery scenario. The prototype's total hardware cost (CAPEX) is approximately €1787, which, when amortized over 3 years and an estimated 1000 flights per year, yields an effective capital cost of €0.60 per flight. Operational expenditures (OPEX) include electricity and maintenance. Each mission consumes about 0.64 kWh, corresponding to an energy cost of €0.13 per kWh, or €0.08 per flight. Preventive maintenance (motors, batteries, frame) is estimated at €250 per year, adding €0.25 per flight. The resulting TCO is therefore ≈ €0.93 per flight, or €0.19 per km for an average 5 km route. In comparison, an electric delivery van operating under similar conditions typically incurs €1.5–2.0 per km, including depreciation and energy, while small combustion vans exceed €2.5 per km. When enabling administrative and regulatory overhead, the UAV achieves a 70–90 % reduction in per-delivery cost and complete elimination of driver-related expenses.

Regarding potential start-up deployment, real-world implementation would require addressing several key challenges: Navigating evolving regulatory frameworks, building public trust in terms of privacy and safety, developing a robust operational infrastructure, and securing sustainable funding. Nonetheless, the proposed system demonstrates technical feasibility and practical relevance, supporting future innovation pathways in sustainable urban mobility and logistics.

4. Discussion

The successful integration of sophisticated embedded algorithms and modern electronic components is what makes this experimental effort successful. The achievement of autonomous flying and optimal energy efficiency depend on this combination's capacity to provide accurate sensing, effective real-time data processing, and intelligent decision-making. Through the use of data-driven modeling and adaptive system resilience, the drone can react to complex and shifting environmental conditions in real time, guaranteeing reliable operation over the mission.

In particular, the embedded system is centered around the NVIDIA Jetson Nano, which

processes sensor data in real-time and executes AI models for route optimization and image enhancement. The system integrates LiDAR, GPS, IMU, and camera inputs, which are processed by Q-learning and CNN modules. A wiring diagram and software architecture overview are provided to illustrate the data flow and component interactions. Performance benchmarks indicate an inference time of ~8 ms for Q-learning and ~250 ms for CNN-based image enhancement, with total power consumption ranging from 3W to 6W under full load.

From a control and navigation standpoint, we examine how advanced AI algorithms can optimize flight paths, prevent collisions, and dynamically adapt to varying environmental conditions. Recent related research further expands the understanding of AI-enabled logistics and UAV optimization. Danach, El Dirani, and Rkein [52] highlighted how artificial intelligence can revolutionize supply chain management by improving both efficiency and sustainability, emphasizing algorithmic decision-making frameworks applicable to large-scale logistics networks. Similarly, Danach et al. [53] proposed location planning techniques for Internet-provider UAVs operating during crises, demonstrating the relevance of AI for real-time service coverage and routing resilience. In contrast, we focus on prototype-level validation and hardware integration, demonstrating how embedded electronics and reinforcement learning algorithms (Q-learning) can translate those conceptual frameworks into a tested, energy-efficient UAV platform. This integration of hardware, AI, and energy-harvesting components complements rather than duplicates the broader system-level perspectives in those studies.

The Q-learning system adopted surpasses traditional route planning methods, achieving a consistent saving in energy consumption and in time flight. The use of these algorithms also increase flight security and the number of avoided collisions. This algorithm is adaptable to changing conditions and continuously improves its navigation decisions through iterative learning. The applicability of a navigation system is tested in a complex urban environment, where it successfully avoids obstacles such as tall buildings and power lines. By optimizing the flight path, the system reduces energy consumption and improved delivery efficiency, achieving a relevant reduction in flight time compared to conventional approaches.

In this case, the software architecture, developed in the ROS 2 environment, includes several dedicated modules. The ekf_fusion node implements an extended Kalman filter that fuses data from GNSS (5–10 Hz), IMU (200 Hz), barometer (50 Hz), and odometric vision (30 Hz), providing a 50 Hz pose estimate as output. The energy_estimator node calculates the instantaneous power P(t) and the energy consumed in Wh using models identified on the test bench, combining the SoC estimate with coulometric integration and OCV curve. The rl_planner node implements tabular Q-learning, which is enriched by a security layer that imposes constraints related to residual energy, wind, and no-fly zones. Finally, the traj_follower node uses a predictive controller (MPC) with a 50 Hz update rate. On the hardware side, critical flight control is handled by an STM32H7 microcontroller, while the reinforcement learning algorithm calculations are performed on a Linux companion computer (Jetson). The power electronics include a 60 A opto-isolated ESC and a 120 A PDB.

Incorporating embedded computing platforms, such as the NVIDIA Jetson Nano, enables real-time processing of data collected from high-precision sensors (GPS, LiDAR sensors, and other electronic components) significantly advancing research into intelligent electronic systems for UAVs.

The development process combined CAD-based conceptual design with physical prototyping and testing. Specifically:

- The drone frame, designed in CAD and printed in PLA reinforced with carbon fibers, isis

tested for structural integrity and payload capacity.

- The electronic integration (ESCs, motors, batteries, Jetson Nano, sensors) is fully assembled and validated through bench testing and flight trials.
- The photovoltaic modules are modeled and dimensioned in CAD, with performance simulated based on manufacturer data; however, in-flight solar harvesting has not been tested experimentally.
- The navigation system (GNSS, INS, LiDAR) and AI algorithms are implemented and tested for real-time telemetry.
- The aerodynamic analysis (e.g., L/D ratio) is derived from semi-empirical models and telemetry, not from CFD or wind tunnel testing.

From an environmental perspective, the combination of electric propulsion, real-time path optimization, and renewable energy integration contribute significantly to reducing greenhouse gas emissions; lowering air and noise pollution and minimizing energy waste. The specific combination of materials and energy source lead to a lower ecological footprint of each delivery, especially compared to traditional combustion-engine vehicles. For this specific reason, a Life Cycle Assessment (LCA) is conducted to quantify the environmental impact of the drone's components. The production of three Tattu 6S 12000mAh LiPo batteries, each rated at 22.2V, results in approximately 959.04 kg of CO_2 emissions, making them the most significant contributor to the drone's carbon footprint. The integration of four perovskite solar modules adds 2.00 kg of CO_2, while the PLA frame, weighing 3.5 kg, contributes only 0.81 kg of CO_2.

When comparing alternative materials for the frame, an ABS structure would emit 4.20 kg of CO_2, and PETG would result in 2.80 kg of CO_2. The total emissions for the drone configuration using PLA are 961.84 kg of CO_2, compared to 965.24 kg with ABS and 963.84 kg with PETG.

These results reinforce the ecological viability of the proposed system, particularly in terms of material selection and energy optimization. The use of biodegradable PLA and high-efficiency components, combined with renewable energy harvesting via perovskite cells, demonstrates a strong commitment to sustainability and low-impact design.

From an economic point of view, the use of autonomous drones powered by AI provides a scalable and economical logistics solution. Reduced energy use, less maintenance, and the removal of personnel costs associated with drivers all contribute to lower operating costs. Furthermore, without the need for substantial infrastructure, drones can access crowded or isolated locations, allowing for quicker service and increased last-mile effectiveness. These elements add to a positive return on investment and make drone logistics especially desirable for applications in smart cities and new companies.

From an urban point of view, all urban flight tests are conducted in compliance with the regulatory framework defined by ENAC (Ente Nazionale per l'Aviazione Civile) and EASA under Reg. (UE) 2019/947 and Reg. (UE) 2019/945. The drone operates within the "Specific Category", requiring prior authorization and risk mitigation measures.

Safety protocols include:

- Geofencing to restrict flight to authorized zones.
- Failsafe mechanisms such as Return-to-Home (RTH), low battery auto-landing, and loss-of-signal procedures.
- Visual Line of Sight (VLOS) maintained at all times.
- Maximum altitude limited to 120 meters.

• Flight permissions are obtained via ENAC's UAS portal, with coordination for BVLOS scenarios where applicable. These measures ensure operational safety and legal compliance during all urban test missions.

During flight operations, several automated failsafe mechanisms are implemented to ensure mission safety and regulatory compliance. In the event of GNSS signal loss, the flight controller automatically switches to inertial and visual odometry–based navigation for up to 5 seconds; if position data remain unavailable beyond this threshold, a Return-to-Launch (RTL) command is triggered, guiding the UAV back to its take-off point using the last valid heading. When the remaining battery energy falls below a predefined threshold (20% state-of-charge) or if both GNSS and IMU data are unreliable, the system initiates an auto-land sequence in a safe, open area. A geofencing system is active throughout each mission, defining horizontal and vertical boundaries (radius 300 m, altitude 120 m) that prevent the drone from entering restricted zones. In addition, a pilot-in-command handover can be activated at any time via the ground control station, enabling manual takeover in Position-Hold mode through the RC transmitter. These layered safety measures, GNSS fallback, automatic failsafe triggers, geofencing, and manual override, significantly enhance the operational robustness of the system during test and real-world missions.

As we look to the future, integrating advanced technologies and ecofriendly materials presents a promising opportunity for urban logistics. For long-term success, it will be essential to invest in research and development to enhance drone performance and minimize their environmental impact. In addition, educating the public about drones' benefits in terms of sustainability and delivery efficiency will help boost acceptance and adoption of these innovative solutions.

5. Conclusions

To enhance the experimental evaluation, particular emphasis was placed on the combination between electronic components and embedded algorithms. This correlation was not only theoretical but actively guided the system design and testing phases, allowing for a more intelligent and adaptive drone behavior. Combining advanced technologies with a strong commitment to environmental protection, is it possible to achieve high efficiency and sustainability. Integrating artificial intelligence, solar energy from perovskite cells, and lightweight materials optimizes performance, reduces energy consumption, and actively reduces CO_2 emissions. This innovative approach demonstrates how technology can be intelligently utilized harmoniously with environmental protection.

We present the first experimental results of integration of electrical components and AI algorithms integrated within the drone, offering promising results. In parallel to these results, it is important to highlight that numerous points of investigation have been found that require further studies. These studies will focus mainly on the development of an *ad hoc* cooling system for the microcontroller and on the improvement of the efficiency of the photovoltaic cells.

The drone's modular components, which lower maintenance costs and provide simple updates, contribute to its economic sustainability in addition to its environmental advantages. Its sophisticated navigation and utilization of renewable energy save operating costs. It enables decentralized, low-impact delivery solutions that are in line with the decarbonization objectives when integrated into a green logistics network.

It can be concluded that the road to a low environmental impact and economic drone for daily

use, well inserted within the urban context, is not very long, but requires further studies and optimizations, in addition to the need to be accepted at city level. Educating the public about the benefits of drone deliveries in terms of efficiency and sustainability will be key to driving acceptance and adoption of these solutions. Transparency in operations and a commitment to responsible business practices will help build consumer trust and solidify the start-up's reputation in the market.

In summary, success in the drone delivery market requires a balance between technological innovation, environmental sustainability, and a solid business strategy.

Author contributions

Conceptualization, L.B., E.G., C.M., S.C., G.B., G.M.M., G.Bi. and V.B.; methodology, L.B., E.G., C.M., S.C., G.B., G.M.M., G.Bi. and V.B.; software, L.B., E.G., C.M., S.C., G.B., G.M.M., G.Bi. and V.B.; validation, L.B., E.G., C.M., S.C., G.B., G.M.M., G.Bi. and V.B.; formal analysis, L.B., E.G., C.M., S.C., G.B., G.M.M., G.Bi. and V.B.; investigation, L.B., E.G., C.M., S.C., G.B., G.M.M., G.Bi. and V.B.; resources, L.B., E.G., C.M., S.C., G.B., G.M.M., G.Bi. and V.B.; data curation, L.B., E.G., C.M., S.C., G.B., G.M.M., G.Bi. and V.B.; writing—original draft preparation, L.B., E.G., C.M., S.C., G.B., G.M.M., G.Bi. and V.B.; writing—review & editing, L.B., E.G., C.M., S.C., G.B., G.M.M., G.Bi. and V.B.; visualization, L.B., E.G., C.M., S.C., G.B., G.M.M., G.Bi. and V.B.; supervision, L.B., E.G., C.M., S.C., G.B., G.M.M., G.Bi. and V.B.; project administration, L.B., E.G., C.M., S.C., G.B., G.M.M., G.Bi. and V.B.; funding acquisition, L.B., E.G., C.M., S.C., G.B., G.M.M., G.Bi. and V.B. All authors have read and agreed to the published version of the manuscript.

Use of Generative-AI tools declaration

The authors declare they have not used Artificial Intelligence (AI) tools in the creation of this article.

Conflict of interest

The authors declare no conflicts of interest

References

1. Gong A, MacNeill R, Verstraete D, Palmer JL (2018) Analysis of a fuel-cell/battery/supercapacitor hybrid propulsion system for a UAV using a hardware-in-the-loop flight simulator. In *2018 AIAA/IEEE electric aircraft technologies symposium (EATS)*, 1–17. https://doi.org/10.2514/6.2018-5017
2. Shiau JK, Ma DM, Yang PY, Wang GF, Gong JH (2010) Design of a solar power management system for an experimental UAV. *IEEE transactions on aerospace and electronic systems* 45: 1350–1360. https://doi.org/10.1109/TAES.2009.5310303
3. Mohanraj D, Aruldavid R, Verma R, Sathiyasekar K, Barnawi AB, Chokkalingam B, et al. (2022) A review of BLDC motor: state of art, advanced control techniques, and applications. *Ieee Access* 10: 54833–54869. https://doi.org/10.1109/ACCESS.2022.3175011
4. Yaşa Y (2022) An efficient brushless DC motor design for unmanned aerial vehicles. *Avrupa*

Bilim ve Teknoloji Dergisi 35: 288–294. https://doi.org/10.31590/ejosat.1083838
5. Deepak B, Singh DP, Kuppa SK, Rao MJ (2023) Design optimization of drone BLDC motor for delivery service applications. *Materials Today: Proceedings*.
6. Emimi M, Khaleel M, Alkrash A (2023) The current opportunities and challenges in drone technology. *Int J Electr Eng Sustain*, 74–89.
7. Barbedo JGA (2019) A review on the use of unmanned aerial vehicles and imaging sensors for monitoring and assessing plant stresses. *Drones* 3: 40. https://doi.org/10.3390/drones3020040
8. Hu T, Sun X, Su Y, Guan H, Sun Q, Kelly M, et al. (2020) Development and performance evaluation of a very low-cost UAV-LiDAR system for forestry applications. *Remote Sensing* 13: 77. https://doi.org/10.3390/rs13010077
9. Rossi M, Brunelli D, Adami A, Lorenzelli L, Menna F, Remondino F (2014) Gas-drone: Portable gas sensing system on UAVs for gas leakage localization. *SENSORS, 2014 IEEE*, 1431–1434. https://doi.org/10.1109/ICSENS.2014.6985282
10. Wei Z, Meng Z, Lai M, Wu H, Han J, Feng Z (2021) Anti-collision technologies for unmanned aerial vehicles: Recent advances and future trends. *IEEE Internet of Things Journal* 9: 7619–7638. https://doi.org/10.1109/JIOT.2021.3135578
11. Harika C, Kumar AS, Rao MR (2024) Comparative Study on Effect of Material on structural Performance of a Quadcopter Drone with 'X-Frame'. In *Journal of Physics: Conference Series* 2837: 012099. IOP Publishing. https://doi.org/10.1088/1742-6596/2837/1/012099
12. Sampaio Saloio JP, Cruz G, Coelho V, N. Torres, JP, Marques Lameirinhas RA (2023) Experimental Study to Increase the Autonomy of a UAV by Incorporating Solar Cells. *Vehicles* 5: 1863–1877. https://doi.org/10.3390/vehicles5040100
13. Pal OK, Shovon M, Mridha M, Shin J (2024) In-depth review of AI-enabled unmanned aerial vehicles: trends, vision, and challenges. *Discover Artificial Intelligence* 4: 1–24. https://doi.org/10.1007/s44163-024-00209-1
14. Annadata YS, Thazhathethil A, Moganarengam V, Nikoubin T (2025) Enhancing Drone-Based Precision Agriculture: Performance Optimization of TinyML Models on Edge Devices and Adaptive Path Planning. *SN Computer Science* 6: 132. https://doi.org/10.1007/s42979-024-03641-3
15. Patnaik A, Michel N, Lin X (2025) Enhancing Multirotor Drone Efficiency: Exploring Minimum Energy Consumption of Forward Flight Under Varying Payload. In *AIAA SCITECH 2025 Forum*, 2187. https://doi.org/10.2514/6.2025-2187
16. 'Il valore dei dati dei droni - Elite Consulting', accessed May 2025. Available from: https://www.eliteconsulting.it/il-valore-dei-dati-dei-droni/
17. Li A, Hansen M, Zou B (2022) Traffic management and resource allocation for UAV-based parcel delivery in low-altitude urban space. *Transportation Research Part C: Emerging Technologies* 143: 103808. https://doi.org/10.1016/j.trc.2022.103808
18. Kumar A, Prybutok V, Sangana VKR (2025) Environmental Implications of Drone-Based Delivery Systems: A Structured Literature Review. *Clean Technologies* **7**: 24. https://doi.org/10.3390/cleantechnol7010024
19. Mitchell S, Steinbach J, Flanagan T, Ghabezi P, Harrison N, O'reilly S, et al. (2023) Evaluating the sustainability of lightweight drones for delivery: towards a suitable methodology for assessment. *Functional Composite Materials* 4: 4. https://doi.org/10.1186/s42252-023-00040-4
20. Bao D, Yan Y, Li Y, Chu J (2025) The Future of Last-Mile Delivery: Lifecycle Environmental

and Economic Impacts of Drone-Truck Parallel Systems. *Drones* 9: 54. https://doi.org/10.3390/drones9010054

21. Park J, Kim S, Suh K (2018) A comparative analysis of the environmental benefits of drone-based delivery services in urban and rural areas. *Sustainability* 10: 888. https://doi.org/10.3390/su10030888
22. Zhou J, Tan L, Liu Y, Li H, Liu X, Li M, et al. (2024) Highly efficient and stable perovskite solar cells via a multifunctional hole transporting material. *Joule* 8: 1691–1706. https://doi.org/10.1016/j.joule.2024.02.019
23. Hailegnaw B, Demchyshyn S, Putz C, Lehner LE, Mayr F, Schiller D, et al. (2024). Flexible quasi-2D perovskite solar cells for energy-autonomous drones. *Nature Energy* 9: 677–690. https://doi.org/10.1038/s41560-024-01500-2
24. Ekrem M, Yılmaz M (2025) Mechanical Properties of PLA, PETG, and ABS. *Necmettin Erbakan Univ. Journal* 7: 161–174.
25. Palade LI, Lehermeier HJ, Dorgan JR (2001) Melt rheology of high L-content poly (lactic acid). *Macromolecules* 34: 1384–1390. https://doi.org/10.1021/ma001173b
26. Tsuji H, Ikada Y (1998) Blends of aliphatic polyesters. II. Hydrolysis of solution-cast blends from poly (L-lactide) and poly (E-caprolactone) in phosphate-buffered solution. *Journal of applied polymer science* 67: 405–415. https://doi.org/10.1002/(SICI)1097-4628(19980118)67:3<405::AID-APP3>3.0.CO;2-Q
27. Hagen R (2000) FIBER RAW MATERIALS-New process to reduce cost price of polylactide. *Chemical Fibers International* 50: 540–541.
28. Linnemann B, Sri Harwoko M, Gries T (2003) FIBER TABLE-Fiber Table Polylactide Fibers (PLA). *Chemical Fibers International* 53: 426–433.
29. Lunt J, Shafer AL (2000) Polylactic acid polymers from com. Applications in the textiles industry. *Journal of Industrial textiles* 29: 191–205. https://doi.org/10.1177/152808370002900304
30. Mahish S, Agarwal V (2001) PLA: Eco-friendly synthetic fibre. *ASIAN TEXTILE JOURNAL-BOMBAY* 10: 42–48.
31. Woodings C (2001) CROP-BASED POLYMERS FOR NONWOVENS. *Nonwovens World* 10: 71–79.
32. Sawyer DJ (2003) Bioprocessing–no longer a field of dreams. *Macromolecular symposia* 201: 271–282. Weinheim: WILEY-VCH Verlag. https://doi.org/10.1002/masy.200351130
33. Dartee M, Lunt J, Shafer A (2000) FIBERS-NatureWorks PLA: Sutainable performance fiber. *Chemical Fibers International* 50: 546–551.
34. Gruber PR, Hall ES, Kolstad JJ, Iwen ML, Benson RD, Borchardt RL (2001) Continuous process for the manufacture of lactide and lactide polymers. U.S. Patent 6,326,458.
35. Mabbrur MAM, Hafidz El Amien N, Syaifer NS, Hidayat A, Nadzir SF (2020) UAV Wing Structure with 3D Printed PLA Filament Wing Spar. *International Journal of Mechanical Engineering and Robotics Research* 9: 464–469. https://doi.org/10.18178/ijmerr.9.3.464-469
36. Ekrem M, Yılmaz M (2025) Mechanical Properties of PLA, PETG, and ABS Samples Printed on a High-Speed 3D Printer. *Necmettin Erbakan Üniversitesi Fen Ve Mühendislik Bilimleri Dergisi* 7: 161–174. https://doi.org/10.47112/neufmbd.2025.83
37. Advantages and Disadvantages of Brushless DC Motors (BLDC) - Arshon Inc. Blog, accessed May 2025. Available from: https://arshon.com/blog/advantages-and-disadvantages-of-brushless-

dc-motors-bldc/
38. Kosovac A, Šabić M, Muharemović E, Šimić E (2022) Shipment delivery challenges using unmanned aerial vehicles. *FIRST INTERNATIONAL CONFERENCE ON ADVANCES IN TRAFFIC AND COMMUNICATION TECHNOLOGIES*, 161–166. https://doi.org/10.59478/ATCT.2022.22
39. Chattopadhyay J, Pathak TS, Santos DM (2023) Applications of polymer electrolytes in lithium-ion batteries: a review. *Polymers* 15: 3907. https://doi.org/10.3390/polym15193907
40. Popa NS, Popescu MO, Mocanu V (2023) State of the Art-Drones/Surface Platforms and Green Energy. In *IOP Conference Series: Earth and Environmental Science*, 012004. https://doi.org/10.1088/1755-1315/1236/1/012004
41. Mulyaningsih TR, Yusuf S, Subehi L, Nugraha MFI, Julzarika A, Sofiyuddin HA, et al. (2023) Determination of heavy metals and rare earth elements in sediment and river water of the Citarum Watershed. In *IOP Conference Series: Earth and Environmental Science* 1221: 012076. IOP Publishing.
42. Zhou J, Tan L, Liu Y, Li H, Liu X, et al. (2024) Highly efficient and stable perovskite solar cells via a multifunctional hole transporting material. *Joule* 8: 1691–1706. https://doi.org/10.1016/j.joule.2024.02.019
43. Rodrigues TA, Patrikar J, Oliveira NL, Matthews HS, Scherer S, Samaras C (2022) Drone flight data reveal energy and greenhouse gas emissions savings for very small package delivery. *Patterns* 3. https://doi.org/10.1016/j.patter.2022.100569
44. Galletta M (2025) Fotovoltaico: nuovo traguardo mondiale. Available from: https://www.tecnoandroid.it/2025/05/09/fotovoltaico-nuovo-traguardo-mondiale-1561682/
45. Kaltenbrunner M, Adam G, Głowacki ED, Drack M, Schwödiauer R, et al. (2015) Flexible high power-per-weight perovskite solar cells with chromium oxide–metal contacts for improved stability in air. *Nature materials* 14: 1032–1039. https://doi.org/10.1038/nmat4388
46. Hailegnaw B, Demchyshyn S, Putz C, Lehner LE, Mayr F, Schiller D, et al. (2024) Flexible quasi-2D perovskite solar cells with high specific power and improved stability for energy-autonomous drones. *Nature Energy* 9: 677–690. https://doi.org/10.1038/s41560-024-01500-2
47. Alarcón F, Viguria A, Vilardaga S, Montolio J, Soley S (2019) EGNOS-based Navigation and Surveillance System to Support the Approval of RPAS Operations. *Proceedings of the 9th SESAR Innovation Days, Athens, Greece*, 2–6.
48. Barrile V, La Foresta F, Genovese E (2024) Optimizing Unmanned Aerial Vehicle Electronics: Advanced Charging Systems and Data Transmission Solutions. *Electronics* 13: 3208. https://doi.org/10.3390/electronics13163208
49. Xu C, Ding W, Lyu W, Liu Z, Wang S, He Y, et al. (2022) Safebench: A benchmarking platform for safety evaluation of autonomous vehicles. *Advances in Neural Information Processing Systems* 35: 25667–25682.
50. Pal OK, Shovon MSH, Mridha MF, Shin J (2024) AI-enabled UAVs: trends, vision, and challenges. *Discov Artif Intell* 4: 1–24. https://doi.org/10.1007/s44163-024-00209-1
51. Kumar A, Prybutok V, Sangana VK (2025) Environmental Implications of Drone-Based Delivery Systems. *Clean Technologies* 7: 24. https://doi.org/10.3390/cleantechnol7010024
52. Danach K, El Dirani A, Rkein H (2024) *Revolutionizing Supply Chain Management with AI: A Path to Efficiency and Sustainability*. IEEE Access. https://doi.org/10.1109/ACCESS.2024.3474531

53. Danach K, Harb H, Rashid ASK, Al-Tarawneh MA., Aly WHF (2025) Location planning techniques for Internet provider service unmanned aerial vehicles during crisis. *Results in Engineering* 25: 103833. https://doi.org/10.1016/j.rineng.2024.103833

AIMS Press